T

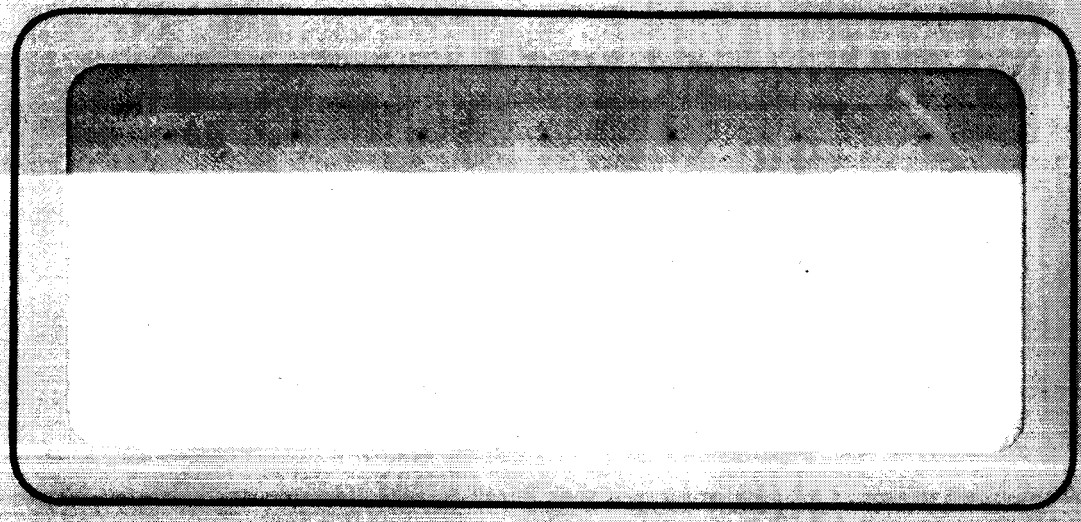

SPACE TECHNOLOGY LABORATORIES, INC.
a subsidiary of Thompson Ramo Wooldridge Inc.
ONE SPACE PARK • REDONDO BEACH, CALIFORNIA

STABILITY OF AXIALLY-LOADED THIN CYLINDRICAL SHELLS UNDER DYNAMIC LATERAL PRESSURES

Final Report on the Buckling of Shells Under Dynamic Loads

by

Leslie R. Koval
James P. O'Neill

EM 13-20 8688-6004-RU000

SPACE TECHNOLOGY LABORATORIES, INC.
A Subsidiary of Thompson Ramo Wooldridge Inc.
One Space Park • Redondo Beach, California

Contract No. NASw-504

October, 1963

Prepared for

THE OFFICE OF GRANTS AND RESEARCH CONTRACTS (SC)
NATIONAL AERONAUTICS AND SPACE ADMINISTRATION
Washington, D. C.

Prepared for
THE OFFICE OF GRANTS AND RESEARCH CONTRACTS (SC)
NATIONAL AERONAUTICS AND SPACE ADMINISTRATION
Washington, D. C.

Prepared: L. R. Koval

L. R. Koval

J. P. O'Neill

Approved: _____

M. V. Barton

SPACE TECHNOLOGY LABORATORIES, INC.
A Subsidiary of Thompson Ramo Wooldridge Inc.
One Space Park · Redondo Beach, California

CONTENTS

ILLUSTRATIONS

TABLES

ABSTRACT

In this report, the results of a theoretical and experimental study of the stability of an axially-loaded thin cylindrical shell under dynamic lateral pressures are presented and discussed. The theoretical study uses nonlinear shallow shell theory to investigate the coupling between an axisymmetric "ring-type" mode and the asymmetric "breathing mode" into which the shell will initially buckle. It is shown that, under certain conditions when the ring mode is dynamically excited, it may be possible to induce buckling at a dynamic critical pressure that is smaller than the static buckling pressure for shells having R/h ratios < 200. A parallel experimental investigation is also reported in which an electrostatic loading system has been developed for the purpose of producing the necessary high rates of loading on the cylinder. This electrostatic loading system was applied to the testing of mylar cylinders.

I. INTRODUCTION

In recent years, increasing attention has been devoted to the buckling of shells under dynamic loading. The motivation for such investigations arises from the concern of designers for the survival of their missiles and spacecraft under conditions of dynamic loading. A common loading condition for a cylindrical shell is a sustained axial compression and a dynamic lateral pressure. Such loadings can arise in missile silo launch, buffeting at transonic speeds, re-entry, and from nuclear blasts outside the atmosphere. The last is a situation which may entail very high rates of loading.

The work reported herein is a continuation of an earlier study[1] and is concerned with the stability of an axially loaded cylindrical shell subjected to axisymmetric dynamic lateral pressure. A complete bibliography of related studies of dynamic buckling would be somewhat long and no attempt will be made to present one here. However, attention is called to related work by Russian and by American authors in 2-22. These works deal with stability of cylindrical shells under both periodic and transients loads.

The primary response to the application of the uniform pressure is an axisymmetric deformation. This inward radially uniform displacement (a "ring-type" mode) induces a circumferential hoop compression, and when this stress reaches a critical value the shell buckles in one of the characteristics asymmetric patterns (a diamond-shaped "breathing mode"). In our earlier study[1], it was shown that if the pressure is applied sufficiently slowly, so that the rise time is large in comparison to the natural period of oscillations of the ring mode, then the dynamic buckling pressure will be the same as the corresponding static value. However, it was hypothesized in this work (suggested by the work of Goodier and McIvor[20] on an infinite cylinder) that a loading time which is shorter than the period of the ring mode would have a critical buckling pressure which might be lower than the static value. Although not strictly correct, this may be conviently described by saying that if the rise time of the load is sufficient to "dynamically excite the ring mode" (considered as a single degree of

freedom linear system), then the dynamic pressure will be lower. It is the purpose of the present work to examine this in greater detail theoretically with a nonlinear analysis. Experiments were also conducted using a new loading technique which permitted the application of loads with rise times shorter than the period of the ring mode. In addition to the stability under transient pressures, oscillatory loads were also studied experimentally.

II. SUMMARY OF RESULTS

A. THEORETICAL STUDY

1) The possibility of a dynamic buckling pressure lower than the static value appears to be a significant design factor only for "thicker" shells ($R/h \leq 200$, especially $R/h \leq 100$) and only under the conditions described below.

2) To show a dynamic effect, the likely static buckling modes must be "tuned" to the axisymmetric "ring-type" mode, i.e., the ratio of frequency of the buckling mode to the frequency of the ring mode must be about 1/2. The degree to which a mode is tuned is critical.

3) For a shell to show a lower dynamic buckling pressure, the dynamic critical pressure for at least one mode must fall below the static buckling pressure of the shell. This is illustrated in Figure 7 and Table 3 of the text.

4) The rise times of the suddenly applied pressures must be shorter than the half-period of the ring mode in order to induce "dynamic buckling."

5) Initial imperfections affect the dynamic buckling pressures to a lesser extent then the static values.

B. EXPERIMENTAL PROGRAM

1) A major effort was expended on the development of an electrostatic system for applying the lateral pressures to the test cylinder. The technique of electrostatically loading structural models is new and its feasibility has been established. Advantages offered by this new procedure are very high rates of loading (measured in microseconds), possibilities for tailoring time histories and spatial distributions of loads, and operation in a vacuum to allow the structural responses to be unimpeded by a fluid in contact with the surfaces.

2) Tests conducted on very thin ($R/h = 800$) mylar cylinders did not detect a difference in buckling pressures between slow and rapid loading rates. This is consistent with theoretical predictions. Thicker shells could not be tested because the necessary pressures for buckling of the cylinder could not be generated electrostatically.

III. THEORETICAL ANALYSIS

The object of the theoretical portion of this study has been to examine the validity of the concept regarding "subcritical" pressures inducing buckling if they are applied to the shell in a sufficiently short increment of time.

A. FORMULATION OF THE PROBLEM

For the purposes of the present study, we employ a nonlinear shallow shell theory analogous to Marguerre's equations for slightly curved plates. In terms of the radial displacement, w, and the stress function, F, appropriate equations have been given by Donnell[23] in the form (see Figure 1 for the coordinate system used)

$$D\nabla^4(w - w_I) + \frac{1}{R}F_{,xx} + \rho h w_{,tt} - F_{,xx}w_{,yy} - F_{,yy}w_{,xx} + 2F_{,xy}w_{,xy} = p(x, y, t) \tag{1}$$

$$\frac{1}{Eh}\nabla^4 F = \left(w_{,xy}^2 - w_{,xx}w_{,yy} - \frac{1}{R}w_{,xx}\right) - \left(w_{I,xy}^2 - w_{I,xx}w_{I,yy} - \frac{1}{R}w_{I,xx}\right) \tag{2}$$

where subscripts following commas denote differentiation. In Equations (1) and (2), w is the total displacement, w_I denotes the initial state of deformation, and D, E, h, R take on the usual meanings (see notation).

Equations (1) and (2) are nonlinear partial differential equations and can be reduced to ordinary nonlinear differential equations by approximate methods such as Galerkin's method or an energy approach using Lagrange's equations. In this study, the latter method is employed and in consequence of this, Equation (1) is not directly used.

The pressures considered here will be assumed to be distributed uniformly over the surface of the shell. Accordingly, the primary shell response is a symmetric radial deformation. However, because of an initially imperfect cylinder, nonsymmetric modes are also excited. One of the objectives of the present study is to examine in detail the coupling between these components of the radial deformation. It is also assumed that the shell is sufficiently long so that the boundary conditions, though still significant, are not critical and the shell is considered simply supported. In view of the preceeding, a solution to Equations (1) and (2)

is assumed to be representable in the form

$$w(x, y, t) = w_o(t) \sin \frac{\pi x}{L} + w_1(t) \sin \frac{m\pi x}{L} \sin \frac{ny}{R} + w_2(t) \sin^2\left(\frac{m\pi x}{L}\right) \tag{3}$$

where $w_o(t)$, $w_1(t)$, and $w_2(t)$ are generalized coordinates. The first term in Equation (3) represents that part of the total response which is due to the axisymmetric ring mode, and the second term represents the breathing mode into which the shell will buckle initially. The last term has been added so as to permit satisfaction of a periodicity condition on the circumferential displacement. The initial deformation pattern of the shell is assumed to be

$$w_I(x, y, t) = u_1 \sin \frac{m\pi x}{L} \sin \frac{ny}{R} + u_2 \sin^2\left(\frac{m\pi x}{L}\right) \tag{4}$$

The second term in Equation (4) is included to satisfy periodicity requirements.

Corresponding to Equations (3) and (4), the stress function F is obtained by solution of Equation (2)

$$\begin{aligned} \frac{F}{Eh} = {} & A_o w_o \sin \frac{\pi x}{L} + A_1(w_1 - u_1) \sin \frac{m\pi x}{L} \sin \frac{ny}{R} \\ & + A_2(w_2 - u_2) \cos \frac{2m\pi x}{L} \\ & + w_o w_1 \left[B_{-1} \cos \frac{(m-1)\pi x}{L} - B_{+1} \cos \frac{(m+1)\pi x}{L}\right] \sin \frac{ny}{R} \\ & + \left(w_1^2 - u_1^2\right)\left(C_1 \cos \frac{2m\pi x}{L} + C_2 \cos \frac{2ny}{R}\right) \\ & + (w_1 w_2 - u_1 u_2)\left(B_3 \sin \frac{3m\pi x}{L} - B_1 \sin \frac{m\pi x}{L}\right) \sin \frac{ny}{R} \end{aligned} \tag{5}$$

where

$$A_o = -\frac{1}{R}\left(\frac{L}{\pi}\right)^2 \quad , \quad A_1 = -\frac{1}{RN_1}\left(\frac{m\pi}{L}\right)^2$$

$$A_2 = \frac{1}{8R}\left(\frac{L}{m\pi}\right)^2 \quad , \quad B_{\pm 1} = \frac{1}{N_{\pm 1}}\left(\frac{\pi}{L}\right)^2\left(\frac{n}{R}\right)^2$$

$$B_3 = \frac{1}{N_3}\left(\frac{n}{R}\right)^2\left(\frac{m\pi}{L}\right)^2 \quad , \quad B_1 = \frac{1}{N_1}\left(\frac{n}{R}\right)^2\left(\frac{m\pi}{L}\right)^2$$

$$C_1 = \frac{1}{32}\left(\frac{n}{R}\right)^2\left(\frac{L}{m\pi}\right)^2 \quad , \quad C_2 = \frac{1}{32}\left(\frac{m\pi}{L}\right)^2\left(\frac{R}{n}\right)^2$$

$$N_1 = \left(\frac{m\pi}{L}\right)^2 + n^2 \quad , \quad N_{\pm 1} = (m \pm 1)^2\left(\frac{\pi}{L}\right)^2 + n^2$$

and

$$N_3 = \left(\frac{3m\pi}{L}\right)^2 + n^2$$

As previously stated, it is necessary to require that the expression for the circumferential component of displacement be periodic, i.e., that the shell remain closed. The last term of Equation (3) has been added to satisfy this requirement. Its form has been selected such as to still permit w to be zero at both edges of the shell. In regard to periodicity, the reader is referred to Reference 24 in which the importance of this condition for dynamic problems is discussed.

The circumferential strain ϵ_y component of an element in the middle surface of the shell is

$$\epsilon_y = \frac{\partial v}{\partial y} + \frac{w}{R} + \frac{1}{2}\left(\frac{\partial w}{\partial y}\right)^2 = \frac{1}{Eh}\left(N_y - \nu N_x\right) \tag{6}$$

where v is the circumferential displacement component

$$N_y = \frac{\partial^2 F}{\partial x^2} = \text{circumferential membrane stress resultant}$$

and

$$N_x = \frac{\partial^2 F}{\partial y^2} = \text{axial membrane stress resultant.}$$

Solving Equation (6) for $\partial v/\partial y$

$$\frac{\partial v}{\partial y} = \frac{1}{Eh}\left(\frac{\partial^2 F}{\partial x^2} - \nu\frac{\partial^2 F}{\partial y^2}\right) - \frac{w}{R} - \frac{1}{2}\left(\frac{\partial w}{\partial y}\right)^2 \tag{7}$$

Substitution of Equations (3), (4) and (5) into Equation (7) and setting to zero the terms that are not harmonic in y leads to the result that

$$\begin{bmatrix} w_2 \\ u_2 \end{bmatrix} = -\frac{n^2}{4R}\begin{bmatrix} w_1^2 \\ u_1^2 \end{bmatrix} \tag{8}$$

The next step in the formulation is the computation of kinetic and potential energies. The kinetic energy is given by

$$T = \frac{1}{2}\rho h\int_0^L\int_0^{2\pi R}\left(\frac{\partial w}{\partial t}\right)^2 dx\, dy \tag{9}$$

where ρ is the mass density and integration is over the surface of the shell. In writing Equation (9), only the energy of the transverse motion is considered on the basis that when the shell buckles, the radial deformation becomes much larger than the other two displacement components. This is identical to considering only transverse inertia and makes the formulation consistent with the shallow shell equations, (1) and (2).

Substituting Equation (3) into Equation (9) and integrating

$$T = \frac{1}{2}\rho h\dot{w}_o^2 I_1 + \frac{1}{2}\rho h\dot{w}_1^2 I_2 + \frac{1}{2}\rho h\left(\frac{n^2}{4R}\right)^2 w_1^2\dot{w}_1^2 I_3 - 2\rho h\left(\frac{n^2}{4R}\right)\dot{w}_o w_1\dot{w}_1 I_4 \tag{10}$$

where dots refer to differentiation with respect to time and

$$I_1 = \pi RL \quad , \quad I_2 = \frac{1}{2}\pi RL \quad , \quad I_3 = \frac{3}{4}\pi RL \quad , \quad \text{and} \quad I_4 = \frac{8m^2}{4m^2 - 1}RL$$

The total potential energy is the sum of the strain energy of the shell, and the work done by the lateral pressure and by the axial load. The strain energy is given by

$$U = \frac{D}{2}\int_0^L\int_0^{2\pi R}\left[\left(\nabla^2 w\right)^2 + 2(1-\nu)\left(w_{,xy}^2 - w_{,xx}w_{,yy}\right)\right] dx\,dy$$

$$+ \frac{1}{2E}\int_0^L\int_0^{2\pi R}\left[\left(\nabla^2 F\right)^2 + 2(1+\nu)\left(F_{,xy}^2 - F_{,xx}F_{,yy}\right)\right] dx\,dy \quad (11)$$

where subscripts refer to differentiation. The first integral is the strain energy due to bending of the shell wall and the second is the contribution from stretching. The details of the substitution of Equations (3) and (5) into Equation (11) are quite complicated and no attempt will be made to present details. Suffice it to record that substitution and integration leads to a result having the form

$$U = w_o^2\left[\frac{D}{2}\left(\frac{\pi}{L}\right)^4 + \frac{Eh}{2}A_o^2\right]I_1 + w_1^2\left[\frac{D}{2}\left(\frac{m^2\pi^2}{L^2} + \frac{n^2}{R^2}\right)^2 + \frac{Eh}{2}A_1^2Q_1^2\right]I_2$$

$$+ K_1 w_o w_1^2 + K_2 w_1^4 + K_3 w_1^6 + K_4 w_o^2 w_1^2 + K_5 w_o w_1^4 + G_1 w_o u_1^2$$

$$- G_2 w_1 u_1 + G_3 w_o w_1 u_1 + G_4\left(w_1 u_1^3 + w_1^3 u_1\right) + G_5 w_1^2 u_1^2$$

$$+ G_6 w_1^3 u_1^3 + G_7 w_o w_1 u_1^3 + (\text{constant terms containing only } u_1) \quad (12)$$

where $K_1, \ldots, K_5$, $G_1, \ldots, G_7$ are extremely complicated coefficients, and

$$Q_1 = \left[\left(\frac{m\pi}{L}\right)^2 + \frac{n^2}{R^2}\right]$$

The work done by the uniform lateral pressure is

$$W_p = -\int_0^L\int_0^{2\pi R} wp\,dx\,dy = -4RLp(t)w_o + \pi RL\left(\frac{n^2}{4R}\right)p(t)w_1^2 \quad (13)$$

There is one final contribution—that due to the axial preload. In this study attention is restricted to the initial stages of instability, in which

case, the work done by the axial load when the shell deflects under the lateral pressure is

$$W_A = \int_0^L \int_0^{2\pi R} \sigma_x^o \left[\frac{\partial u}{\partial x} + \frac{1}{2}\left(\frac{\partial w}{\partial x}\right)^2 \right] dx\, dy \tag{14}$$

where the initial axial stress induced by the axial load P is

$$\sigma_x^o = \frac{P}{2\pi R h}$$

Finally, application of Lagrange's equations

$$\frac{d}{dt}\left(\frac{\partial T}{\partial \dot{w}_i}\right) - \frac{\partial}{\partial w_i}(T - U + W_p + W_A) = 0, \quad i = 0, 1 \tag{15}$$

leads to the coupled nonlinear ordinary differential equations

$$\begin{aligned} &\ddot{w}_o + w_o\left(\Omega_o^2 + a_1 w_1^2\right) + a_2 w_1^2 + a_3 w_1^4 - a_4\left(w_1 \ddot{w}_1 + \dot{w}_1^2\right) \\ &\qquad + \left(\gamma_3 u_1 + \frac{1}{2}\gamma_7 u_1^3\right) w_1 = -a_5 p(\tau) - \gamma_1 u_1^2 \\ &\ddot{w}_1\left(1 + \beta_8 w_1^2\right) + w_1\left\{\left[\Omega_1^2 + \gamma_5 u_1^2 - \beta_5 p(\tau)\right] + \beta_1 w_o^2 + \beta_2 w_o^2 + \beta_3 w_o w_1^2\right. \\ &\qquad \left. + \beta_8 \dot{w}_1^2 + \beta_4 \ddot{w}_o - 3\gamma_4 u_1 w_1 - \gamma_6 u_1^3 w_1\right\} \\ &\qquad + \beta_6 w_1^3 + \beta_7 w_1^5 = \gamma_2 u_1 - 2\gamma_3 u_1 w_o + \gamma_4 u_1^3 - \gamma_7 u_1^3 w_o \end{aligned} \tag{16}$$

where w_o, w_1, and u_1 have been non-dimensionalized with respect to wall thickness, time is non-dimensionalized on the ring mode according to

$$\tau = ct \quad , \quad c^2 = E/\rho R^2$$

and

$$\Omega_1^2 = 1 + \frac{k}{1 - \nu^2}\left(\frac{\pi}{\ell}\right)^4 - \frac{P}{2\pi RhE}\left(\frac{\pi}{\ell}\right)^2$$

$$\Omega_2^2 = \frac{1}{N_1^2}\left(\frac{m\pi}{L}\right)^4 + \frac{k}{1 - \nu^2} N_1^2 - \frac{P}{2\pi RhE}\left(\frac{m\pi}{\ell}\right)^2$$

$$a_1 = \frac{3}{2} kn^4\left(\frac{\pi}{\ell}\right)^4\left(\frac{1}{N_{-1}^2} + \frac{1}{N_{+1}^2}\right)$$

$$a_2 = \frac{1}{2\pi}\left\langle \frac{k}{1 - \nu^2} n^2 \frac{h}{R}\left(\frac{\pi}{\ell}\right)^4 \frac{4m^2}{4m^2 - 1} + \frac{2(1 + \nu)}{N_1^2}\frac{h}{R} n^4\left(\frac{\pi}{\ell}\right)^4 \right.$$

$$\left[\frac{(m - 1)\frac{\pi}{\ell}\frac{2m - 2}{2m - 1}}{N_{-1}^2} + \frac{(m + 1)\frac{\pi}{\ell}\frac{2m + 2}{2m - 1}}{N_{+1}^2}\right]$$

$$+ \frac{h}{R} n^2 \frac{\left(\frac{m\pi}{\ell}\right)^2\left(\frac{\pi}{\ell}\right)^2}{N_1^2}\left[\frac{2m}{N_{-1}^2(2m - 1)} + \frac{2m}{N_{+1}^2(2m + 1)}\right]$$

$$- (1 + \nu)\frac{h}{R}\frac{n^4}{N_1^2}\left(\frac{m\pi}{\ell}\right)^2\left(\frac{\pi}{\ell}\right)^2\left\{\frac{2m}{N_{-1}^2(2m - 1)}\left[(m - 1)^2\frac{\pi^2}{\ell^2} + \left(\frac{m\pi}{\ell}\right)^2\right]\right.$$

$$\left.\left. + \frac{2m}{N_{+1}^2(2m + 1)}\left[(m + 1)^2\frac{\pi^2}{\ell^2} + \left(\frac{m\pi}{\ell}\right)^2\right]\right\}\right\rangle$$

$$a_3 = \left(\frac{h}{R}\right)^3 \frac{n^6}{8\pi}\left(\frac{m\pi}{\ell}\right)^2\left(\frac{\pi}{\ell}\right)^2$$

$$\left\langle \frac{1}{N_3^2}\left[\frac{12m}{N_{-1}^2(2m+1)(4m-1)} - \frac{12m}{N_{+1}^2(2m-1)(4m+1)}\right]\right.$$

$$- \frac{1}{N_1^2}\left[\frac{2m}{N_{+1}^2(2m+1)} - \frac{2m}{N_{-1}^2(2m-1)}\right]$$

$$+ \frac{24(1+\nu)m}{N_3^2}\left(\frac{\pi}{\ell}\right)^2\left[\frac{(m-1)^2}{N_{-1}^2(2m+1)(4m-1)} - \frac{(m+1)^2}{N_{+1}^2(2m-1)(4m+1)}\right]$$

$$- \frac{4(1+\nu)m}{N_1^2}\left(\frac{\pi}{\ell}\right)^2\left[\frac{(m-1)^2}{N_{-1}^2(2m-1)} + \frac{(m+1)^2}{N_{+1}^2(2m+1)}\right]$$

$$+ (1+\nu)\left(\frac{\pi}{\ell}\right)^2 n^2\left\{\frac{12m}{N_3^2}\left[\frac{(m+1)^2+9m^2}{N_{+1}^2(2m-1)(4m+1)} - \frac{(m-1)^2+9m^2}{N_{-1}^2(2m+1)(4m-1)}\right]\right.$$

$$\left.\left. + \frac{2m}{N_1^2}\left[\frac{(m+1)^2+m^2}{N_{+1}^2(2m+1)} + \frac{(m-1)^2+m^2}{N_{-1}^2(2m-1)}\right]\right\}\right\rangle$$

$$a_4 = \frac{1}{\pi}\frac{h}{R}n^2\frac{4m^2}{4m^2-1}$$

$$a_5 = \frac{4}{3\pi}\frac{1}{Ek}$$

$$\beta_1 = 4a_2$$

$$\beta_2 = 3k\left(\frac{\pi}{\ell}\right)^4 n^4\left(\frac{1}{N_{-1}^2} + \frac{1}{N_{+1}^2}\right)$$

$$\beta_3 = 8a_3 \quad , \qquad \beta_4 = 2a_4 \quad , \qquad \beta_5 = \frac{n^2}{E\left(\frac{h}{R}\right)}$$

$$\beta_6 = 48k\left(\frac{m\pi}{\ell}\right)^4\left[\frac{1}{64} - \frac{n^4}{4N_1^2} + \frac{n^4k}{4(1-\nu^2)}\right] - \frac{3P}{2\pi RhE}\left(\frac{m\pi}{\ell}\right)^2 n^4k$$

$$\beta_7 = 27k^2n^8\left(\frac{m\pi}{\ell}\right)^4\left(\frac{1}{N_3^2} + \frac{1}{N_1^2}\right)$$

$$\beta_8 = \frac{9}{2}n^4k$$

$$\gamma_1 = \frac{1}{2}\frac{h}{R}\frac{n^2}{4m^2 - 1}$$

$$\gamma_2 = \left(\frac{m\pi}{\ell}\right)^4\frac{1}{N_1^2}$$

$$\gamma_3 = \frac{n^2}{N_1}\frac{h}{R}\left(\frac{m\pi}{\ell}\right)^2\left(\frac{\pi}{\ell}\right)^2$$
$$\left\{-\left[\frac{2m}{N_{-1}^2(2m-1)} + \frac{2m}{N_{+1}^2(2m+1)}\right]\right.$$
$$+ \frac{1+\nu}{2}\frac{n^2}{N_1^2}\left(\frac{\pi}{\ell}\right)^2\left[\frac{2m}{N_{-1}^2(2m-1)}\right.$$
$$\left.\left. + \frac{2m}{N_{+1}^2(2m+1)} + \frac{4m(m-1)}{N_{-1}^2(2m-1)} + \frac{4m(m+1)}{N_{+1}^2(2m+1)}\right]\right\}$$

$$\gamma_4 = 3kn^4\left(\frac{m\pi}{\ell}\right)^4\frac{1}{N_1^2}$$

$$\gamma_5 = \frac{3}{2}kn^4$$

$$\gamma_6 = 27k^2n^8\left(\frac{m\pi}{\ell}\right)^4\left\{\frac{1}{N_3^2} + \frac{1}{N_1^2} + 2(1+\nu)\left[\frac{\left(\frac{3m\pi}{\ell}\right)^2 n^2}{N_3^2} + \frac{\left(\frac{m\pi}{\ell}\right)^2 n^2}{N_1^2}\right]\right\}$$

$$\gamma_7 = \left(\frac{h}{R}\right)^3 \frac{n^6}{4\pi}\left(\frac{m\pi}{\ell}\right)^2\left(\frac{\pi}{\ell}\right)^2$$

$$\left\langle \frac{1}{N_3^2}\left[-\frac{12m}{N_{-1}^2(2m+1)(4m-1)} + \frac{12m}{N_{+1}^2(2m-1)(4m+1)}\right]\right.$$

$$+ \frac{1}{N_1^2}\left[\frac{2m}{N_{-1}^2(2m-1)} + \frac{2m}{N_{+1}^2(2m+1)}\right]$$

$$+ 2(1+\nu)\left(\frac{m\pi}{\ell}\right)n^2\left\{\frac{3\frac{\pi}{\ell}}{N_3^2}\left[\frac{(m-1)^2}{N_{-1}^2(2m+1)(4m-1)} - \frac{(m+1)^2}{N_{+1}^2(2m-1)(4m+1)}\right]\right.$$

$$\left. - \frac{2\frac{\pi}{\ell}}{N_1^2}\left[\frac{(m-1)^2}{N_{-1}^2(2m-1)} + \frac{(m+1)^2}{N_{+1}^2(2m+1)}\right]\right\}$$

$$+ (1+\nu)n^2\left\{\frac{12m}{N_3^2N_{-1}^2(2m+1)(4m-1)}\left[\left(\frac{3m\pi}{\ell}\right)^2 + (m-1)^2\frac{\pi^2}{\ell^2}\right]\right.$$

$$- \frac{2m}{N_1^2N_{+1}^2(2m+1)}\left[\left(\frac{m\pi}{\ell}\right)^2 + (m+1)^2\frac{\pi^2}{\ell^2}\right]$$

$$+ \frac{2m}{N_1^2N_{-1}^2(2m-1)}\left[\left(\frac{m\pi}{\ell}\right)^2 + (m-1)^2\frac{\pi^2}{\ell^2}\right]$$

$$\left.\left. - \frac{12m}{N_3^2N_{+1}^2(2m-1)(4m+1)}\left[\left(\frac{3m\pi}{\ell}\right)^2 + (m+1)^2\frac{\pi^2}{\ell^2}\right]\right\}\right\rangle$$

$$k = \frac{h^2}{12R^2}$$

and

$$\ell = \frac{L}{R}$$

Clearly, Equation (16) is too difficult for an analytical solution and recourse was made to a digital computer program in which a finite difference scheme was used having a variable step size. This step size was continuously picked as part of the program so as to keep the pointwise error within specified limits.

Before proceeding to discuss these computations, it is possible to make some observations which will help in the understanding and interpretation of the numerical results. If Equations (16) are linearized, and the initial imperfections taken to be very small, then one obtains the set of equations

$$\ddot{w}_o + \Omega_o^2 w_o = -a_5 p(\tau) \tag{17}$$

$$\ddot{w}_1 + w_1\left[\Omega_1^2 - \beta_5 p(\tau) + \beta_1 w_o + \beta_4 \ddot{w}_o\right] = 0 \tag{18}$$

Equation (17) suggests that the initial response to the pressure is a pure radial deformation* which, in turn, parametrically excites the breathing mode (note that this requires an initial value for w_1 so that initial imperfections are required to trigger the phenomenon). In the case of a slowly varying load, the inertia term in Equation (17) can be neglected and the solution to Equation (17) is

$$w_o = -\frac{a_5}{\Omega_o^2} p(\tau) \tag{19}$$

so that Equation (18) can be written as

$$\ddot{w}_1 + \left[\Omega_1^2 - \beta_5 p(\tau) - \frac{\beta_1 a_5}{\Omega_o^2} p(\tau)\right] w_1 = 0 \tag{20}$$

Equations (19) and (20) constitute the analysis previously carried out in Reference 1. The critical linearized static buckling pressure is

*This, of course, is consistent with the assumption in Equation (3).

$$\left(p_{cr}\right)_{linearized} = \frac{\Omega_1^2 \Omega_o^2}{\beta_1 a_5 + \beta_5 \Omega_o^2} \tag{21}$$

and this was used in this investigation to estimate the critical pressure under slow rates of loading. Numerical calculations indicated that Equation (21) provides very satisfactory accuracy. Comparison with experimental results of Weingarten, Morgan and Seide,[27] for buckling under hydrostatic pressure also indicates reasonably good accuracy. It also gives values consistent with experimental results of Reference 1. Equation (21) does not contain the effects of initial imperfections, but doing so leads to the result that

$$\left(p_{cr}\right)_{linearized} = \frac{\Omega_1^2 \Omega_o^2 - \beta_1 \gamma_1 u_1^2}{\beta_1 a_5 + \beta_5 \Omega_o^2} \tag{22}$$

In using Equation (21) or (22), the quantity of interest is the smallest value of p_{cr}. The usual procedure for finding this is to examine all the possible buckling modes and pick that combination of (m, n) which minimizes p_{cr}. This minimum value is the critical buckling pressure for the shell and the corresponding values of (m, n) determine the mode into which the shell will buckle, i.e., the "buckling mode."

When the pressure is dynamically applied, such as an instantaneous jump to a value p_o, then the solution of Equation (17) (for this step pressure) is

$$w_o = -\frac{a_5 p_o}{\Omega_o^2}\left(1 - \cos \Omega_o t\right) \tag{23}$$

Substituting Equation (23) into Equation (18) yields

$$\ddot{w}_1 + \left(a - 2q \cos \Omega_o t\right) w_1 = 0 \tag{24}$$

where

$$a = \Omega_1^2 - \frac{\beta_5 \Omega_o^2 + \beta_1 a_5}{\Omega_o^2} p_o$$

and

$$2q = p_o\left(\frac{\beta_1 a_5}{\Omega_o^2} + a_5\beta_4\right)$$

Equation (24) is Mathieu's equation[28] indicating that in the linear theory, stability under suddenly applied pressures is of the Mathieu type. In this type of parametric resonance, the most important unstable region occurs for $\Omega_1 = (1/2)\Omega_o$. This implies that the modes into which the shell is most likely to buckle dynamically are those modes which have their natural frequencies equal to about one-half of the frequency of the ring mode.

On the basis of this linearized analysis, attention will be focused on those modes which are "tuned" to the ring mode as indicated above.

B. NUMERICAL CALCULATIONS

In the numerical calculations, the suddenly applied pressure is represented by the "ramp-step" pressure-time curve of Figure 2a, for which τ_1 is the nondimensionalized rise time and p_o is the eventual magnitude of load. The limit $\tau_1 \rightarrow 0$ represents a load which is instantaneously applied, and a large τ_1 corresponds to a slow rate of loading. Also considered briefly is a "rectangular" pulse, Figure 2b, characterized by the instantaneous application of pressure which is maintained at p_o until time τ_2 when it is suddenly removed. The time τ_2 is the duration of the pulse, and the limiting case $\tau_2 \rightarrow 0$, represents a purely impulsive load.

Results were obtained for two classes of shells. The first was a very thin shell having a length equal to 8 inches, a radius of 4 inches, and a thickness of 0.005 inch, which is subjected to a 30 pound axial load. These numbers correspond to the cylinder which was tested in a series of laboratory experiments. The second group of cylinders had L/R = 1 with R/h varying from R/h = 200 down to R/h = 50. There was no axial load in this case. In both sets of calculations, the shell material was mylar with $E = 0.735 \times 10^6$ psi and $(E/\rho)^{1/2} = 7.53 \times 10^4$ in/sec. Unless specifically stated otherwise, u_1 has been taken as 1 percent of the thickness, i.e., $u_1 = 0.01$. Emphasis during the numerical work has been placed on determining trends rather than data for detailed design curves.

1. Determination of "Buckling" and the Existence of "Dynamic Buckling"

In all cases buckling was determined as that value of p_o for which the character of the resulting motion abruptly changed from a state of small or moderate deformation to one of large deformation.* Typical examples of this are presented in Table 1 and graphically illustrated in Figure 3 for the ramp-step pressure loading. The values $\tau_1 = 0.001$ and 50 represent fast and slow rates of loading, respectively. Inspection of Table 1 indicates that the modal critical pressures for the mode m = 7, n = 11 is $p_o = 1.56$ when the load is applied very slowly, but decreases to $p_o = 0.71$ if the pressure is very suddenly applied. Thus, the shell will buckle in this mode at a lower pressure if the loading rate is fast enough. This result is analogous to results obtained by Budiansky and Roth[25] who found a decrease of 1/3 for a shallow spherical shell. Hoff and Bruce[26] found a decrease of 22 percent for a slightly curved bar.

In contrast, there is no difference in buckling pressures for the mode m = 1, n = 10, both giving values of 0.0118. It is of interest to observe that Equation (21) predicts static buckling pressures of 1.61 and 0.0117, which indicates that the jump to large deformations is a valid criteria for buckling.

The mode (7, 11) has for the ratio of the natural frequency of its small oscillations (Ω_1) to the corresponding frequency of the ring mode (Ω_o) a value of 0.468, and the mode (1, 10) has $\Omega_1/\Omega_o = 0.036$. The above critical pressures suggest that if the breathing mode is "tuned"** to the ring mode, then the pressure required to buckle a cylinder in that mode when the pressure is very suddenly applied may be less than the corresponding critical pressure under static loads. In contrast, those modes which are not tuned (such as m = 1, n = 10) will not show appreciably different dynamic and static critical pressures. Comparison of the modal buckling pressures for these two modes clearly indicates that the

*A similar criteria was used by Budiansky and Roth[25] in their study of the axisymmetric dynamic buckling of a clamped shallow spherical shell, and by Roth and Klosner[22] who studied a thin cylinder under a sudden axial load.

**"Tuning" will mean a frequency ratio of about 1/2 as per linear theory.

shell will buckle in the (1, 10) mode rather than (7, 11). As regards the overall shell stability the critical buckling pressure for the shell consequently will not indicate any dynamic effect. Only if the decreased pressure for the tuned mode falls below that of the untuned mode could the shell buckle at a smaller dynamic pressure. In this situation, the initial dynamic buckling mode would be different from the static one. Since this study is restricted to the initial stages of buckling, it is not possible to comment on the final post buckling configuration under conditions of slowly or rapidly applied pressures.

Table 1. Maximum Amplitude of Response for Typical Modes for R/h = 800, L/R = Z, P = 30 Pounds, $u_1 = 0.01$

Mode	Ω_1	τ_1	p_o	$w_{1,max}$
m = 1, n = 10	0.036	50	0.010	0.054
			0.011	0.137
			0.0115	0.499
			0.01175	0.600
			0.0118	6.63†
			0.012	17.0
			$(P_{cr})_{static}$	$\cong$ 0.0118
		0.001	0.010	0.046
			0.011	0.109
			0.0115	0.248
			0.0118	6.56†
			0.012	16.98
			$(P_{cr})_{dynamic}$	$\cong$ 0.0118
m = 7, n = 11	0.468	50	1.50	0.246
			1.55	0.543
			1.556	0.649
			1.5625	24.4*
			1.575	24.5
			1.70	24.6
			$(P_{cr})_{static}$	$\cong$ 1.56
		0.001	0.60	4.03
			0.70	4.45
			0.707	4.81
			0.715	24.4**
			0.75	25.7
			0.80	24.2
			$(P_{cr})_{dynamic}$	$\cong$ 0.71

*went unstable at τ = 160

**went unstable at τ = 140

†went unstable at τ = 154

These preliminary results clearly show the possibility of a "premature" dynamic critical pressure, but also show the limitations on its being a significant design consideration. It would appear that this phenomenon is practically important only for those shells having likely buckling modes which are tuned to the ring mode. As we shall presently see, this restricts attention to thicker shells.

Before proceeding, it should be remarked that the mode (1, 10) was picked in the above computation because it was that mode which had the smallest static critical pressure as determined from Equation (21). The mode (7, 11) was chosen because preliminary tests indicated that the final buckled configuration had n = 11 circumferential waves. The mode with n = 11 having its frequency approximately half the ring mode frequency has 3-1/2 axial waves (m = 7) and it was decided to determine the existence of a lower dynamic critical pressure using this mode. It was later found that the mode (1, 36) showed a more striking effect (see Table 4), but parameter studies had already been started on (7, 11).

2. Characteristics of the Phenomenon

Having established the theoretical existence of a "dynamic buckling" phenomenon, it is of considerable interest to examine its character in more detail. Of prime interest is the effect of the rise time of the load, i.e., how fast must the load be applied so that the shell will buckle at a smaller critical pressure?

Figure 4 shows the result of varying the rise time τ_1 for the mode (7, 11). The abscissa represents the extent to which the loading has a dynamic character. If one considers the ring mode from the point of view of Equation (17), and takes $p(\tau)$ as in Figure 2a, the linearized ring mode response is then

$$w_o = -\frac{a_5 p_o}{\Omega_o^2}\left[1 - \eta \cos \Omega_o \tau\right] \tag{25}$$

where

$$\eta = \frac{2}{\tau_1}\left|\sin \frac{1}{2}\tau_1\right|$$

For a rise time $\tau_1 \rightarrow 0$, $\eta \rightarrow 1$ and this is the maximum dynamic effect created by the sudden application of the external pressure. For very slow rates of loading, $\tau_1 \rightarrow \infty$ and $\eta \rightarrow 0$. This is the case of static loading. As shown in Figure 4, there is no decrease in critical pressure unless the rise time is less than half the natural period (which is π in terms of τ) of the ring mode.

3. Initial Imperfections

Since most structures are not "perfect," i.e., do not conform to the mathematical idealizations employed, it is also of interest to examine the effect of deviations of the actual structure from the ideal. In the case of shells, this is treated by the introduction of the concept of "initial imperfections" which represent the degree by which the initial shape of the shell deviates from a perfect cylinder. Figure 5 shows the result of a change in the initial imperfection on the buckling pressures for the mode n = 7, n = 11. The imperfections u_1, have been nondimensionalized on the wall thickness h. It is interesting to observe that imperfections appear to have a much greater effect under slow rates of loading than they do under high rates. Attention is also called to the tendency of larger imperfections to bring the two curves together. This seems to imply that a poorly made cylinder will show a smaller decrease in dynamic critical pressure than would a better specimen, chiefly because of the degradation in static buckling pressure.

4. Thicker Shells

A second set of calculations were made in a search for cylinders of practical dimensions for which dynamic buckling considerations are important. Based on the calculations described above, it was apparent that the shell geometry must be such that the likely static buckling modes are tuned to the ring mode and this implied that the R/h ratio must be larger. Accordingly, a series of calculations were made for shells in the range

$$50 \leq R/h \leq 200$$

and having L/R = 1. The general results can be extended to longer shells if it is observed from the definition of Ω_1 and Ω_o in Equation (16) that an increase in L/R implies a smaller R/h (i.e., larger k) in order to maintain the proper ratio between Ω_1 and Ω_o for a given mode. Again, buckling has been taken as the change in deformation from small to large values, as illustrated for a typical case in Table 2. Table 3 presents a summary of the calculations for three rise times:

Virtually instantaneous	$\tau_1 = 0.001$
Fast, but finite, rise time	$\tau_1 = 2.25$
Slow	$\tau_1 = 50$

The reason for inclusion of the intermediate value of τ_1 is the desire to include a fast rise time that is more realistic than an instantaneous application of load. The value $\tau_1 = 2.25$ is still quite fast for it represents a rise time of about two-thirds the natural half-period of the ring mode. In the case of a R = 4 inch mylar cylinder, this is a rise time of about 120 microseconds. Inspection of Table 3 indicates that buckling under "subcritical" dynamic loads is a design consideration only for those shells having $R/h < 200$, especially for $R/h < 100$. It does not appear that thinner shells will show any difference in the shell's buckling pressure under fast or slow rates of loading for the reasons discussed earlier.

In Table 3, the modes given are those modes having the smallest critical pressures, although it was necessary to examine a number of modes for each shell geometry.

Before leaving Table 3, it is noteworthy that the magnitude of the decrease in critical pressure appears to vary with the frequency ratio Ω_1/Ω_o. Further insight into this aspect can be obtained by inspection of Table 4 and Figure 6 which clearly indicate the existence of an "optimum" tuning between breathing mode and ring mode. This is due to the fact that the phenomenon under study is one of parametric resonance (analysis with the linearized equations lead to Mathieu's equations). The ring mode is excited by the application of pressure and this in turn drives the breathing mode parametrically. The sharp dip in the neighborhood of $\Omega_1/\Omega_o = 0.5$ is directly related to the first unstable region in a stability diagram for

Table 2. Maximum Amplitude of Response for Critical Modes for R/h = 100, L/R = 1

τ_1	Mode	p_o	$w_{1\ max}$	$w_{o\ max}$
50	m = 1, n = 8	7.30	5.64	2.19
		7.70	4.80	1.07
		7.705	16.4	70
		7.75	16.9	92
		7.80	16.8	80
0.001	m = 1, n = 12	1.05	2.4	2.4
		1.055	5.0	6.4
		1.0625	12.9	91
		1.075	12.9	102
		1.100	12.9	103
$(p_{cr})_{static} = 7.70$, $(p_{cr})_{dynamic} = 1.06$				

Table 3. Critical Pressures for Thicker Shells

R/h	Ω_1/Ω_o	Mode	Loading Rate, τ_1	Critical Pressure	
					% of static
200	0.226	m = 1, n = 10*	50	1.25	--
	0.506	m = 1, n = 18	0.001	0.15	12
			2.25	1.25	100
100	0.260	m = 1, n = 8*	50	7.70	--
	0.469	m = 1, n = 12	0.001	1.06	14
			2.25	1.66	21
75	0.290	m = 1, n = 7*	50	13.86	--
	0.533	m = 1, n = 11	0.001	1.12	8
			2.25	1.15	9
50	0.350	m = 1, n = 6*	50	37.3	--
	0.466	m = 1, n = 8	0.001	6.1	16
			2.25	25.0	67

*Static buckling mode

Mathieu's equation[28]. The effect of the nonlinearity is to modify the value of Ω_1/Ω_o at which the dip occurs and make it dependent on shell geometry, as is evident in comparing Tables 3 and 4. Although damping has not been considered in this study, inclusion of its effects would probably decrease the depth of the dip, thereby raising the critical pressures under dynamic loads. In Figure 7 are plotted the static and dynamic buckling curves which were used to construct Figure 6, and these curves strikingly illustrate that although an individual mode may show a significant decrease in dynamic buckling pressure, the shell will still buckle as if under static load if the minimum dynamic buckling pressure is higher than the minimum static pressure. In Figure 7, the dynamic buckling pressure of the mode (1, 36) is still higher than the static buckling pressure for (1, 10) so that the shell will buckle in (1, 10) under both and dynamic pressures. To have dynamic buckling occur, it is necessary for the dynamic buckling pressure of one of the tuned modes to fall below the critical pressure of the mode in which the shell will buckle under statically applied pressures.

Table 4. The Effect of Tuning on Dynamic Buckling Pressure for R/h = 800, L/R = 2, P = 30 Pounds

Mode	Ω_1/Ω_o	p_{st}	p_{dyn}	p_{dyn}/p_{st}
m = 1, n = 10	0.036	0.0118	0.0118	1.00
m = 6, n = 11	0.396	1.15	1.07	0.93
m = 7, n = 11	0.468	1.56	0.71	0.46
m = 1, n = 36	0.490	0.178	0.015	0.08
m = 6, n = 9	0.499	2.62	0.66	0.26

Figure 6 also helps explain the apparent nonuniformity in the behavior of the variation of the dynamic critical pressure with shell geometry. It is apparent that each class of shell geometry has associated with it a curve similar to the solid curve in Figure 6 and each mode of that shell will have a frequency ratio corresponding to a point on the curve (however, each point on the curve does not correspond to a shell mode because the shell modes have integral values of m, n only). It

would appear entirely possible that a given shell could have frequency ratios that miss the deepest part of the dip and thereby not demonstrate a difference in static and dynamic critical pressures to the extent that another (and maybe thinner) shell might. This seems to be the case in Table 3.

5. Time for the Buckling Process

From inspection of the numerical runs, it is possible to estimate the time required for the cylinder to buckle in those cases when an instability did occur. An interesting correlation with experimental observations can then be made. The time at which buckling (i.e., large deformations) occurred fell in a broad band which depended on the mode, shell geometry and load. Generally speaking, however, it fell in the range $50 < \tau < 250$ which corresponds to buckling times of $0.003 < t < 0.015$ second. A very typical value was about $\tau = 150$ ($t = 0.008$ second). This number seems to be in good agreement with times observed by Tennyson[29] of 0.006 second for an axially compressed cylinder and by Evensen[30] of about 0.007 second for hydrostatic compression and 0.004 for axially compressed cylinders. While there is bound to be discrepancies in the exact values of the buckling times because of difficulties in determining starting times for the phenomenon, it is encouraging to note the agreement on the order of magnitude. It is also of interest to note that these times correspond to something on the order of 25 cycles of the ring mode.

6. Impulsive Loads

By use of the rectangular pulse in Figure 2b, preliminary computations were made on the response of a representative mode to an impulsive pressure. As with many of the numerical calculations, the mode $m = 7$, $n = 11$ for the very thin cylinder was used. The result is presented below in Table 5 and both critical pressure and critical impulse are plotted in Figure 8. The dotted portion of the critical impulse curve has been faired-in.

Table 5. Stability Under Impulsive Pressures
R/h = 800, L/R = 2, P = 30 pounds,
m = 7, m = 11

τ_2	p_{cr}	Impulse	Remarks
3.5	0.71	2.475	Essentially a maintained load.
1.0	0.715	0.715	---
0.54	1.01	0.545	True impulsive loads.
0.27	2.01	0.543	
0.10	4.25	0.425	
0.05	10.00	0.500	

One can observe the well known result that a supercritical load can be applied without leading to collapse if the load is removed sufficiently soon. It is also interesting to note that in the case of very short durations, the governing factor on buckling appears to be the impulse given to the shell. A similar curve was also obtained by Budiansky and Roth[25] and by Roth and Klosner[22]. The reader is reminded that the rectangular pulse used here has zero rise time, consequently the horizontal asymptote of the critical pressure curve is the critical pressure for a suddenly applied pressure rather than that for static loading.

IV. THE EXPERIMENTAL PROGRAM

During the experimental portion of the earlier program[1], a 3 millisecond rise time for the step pressures was obtained with a light-weight specially designed evacuating piston which was essentially a high-frequency, but long-stroke, loudspeaker mechanism. This loading rate was fast enough to excite the buckling modes of an 8 inch diameter mylar cylinder, but not fast enough to excite the cylinder's 3000 cps ring mode. In these tests, it was observed that the dynamic critical collapse pressure was not significantly different from the static value.

The principal objective of the present experimental program was to devise an experimental procedure for exciting the ring mode and to look for the different collapse pressures that might result.

Two basic methods of achieving a loading rate fast enough to excite the ring mode were evaluated at the beginning of this investigation. The first was to accept the 3-millisecond rise time developed by air pressure loading and to develop a cylindrical shell with a lower ring-mode frequency. The other was to retain the thin-walled, cylindrical mylar test specimen and to excite the 3000 cps ring mode with electrostatically applied radial pressures. The elctrostatic-loading route was chosen for development because 1) calculations showed adequate load capability for testing mylar cylinders and showed more than adequate loading-rate capability, 2) no practical isotropic material have an adequately low ring-mode frequency could be found and composite structures (such as lead-shot filled jelly-like plastics) which did have a low ring mode frequency do not simulate the thin-walled type of structure that is of primary interest, and 3) extensive experience with mylar as a material for shell buckling experiments had shown it capable of reproducible results during repeated buckling tests on the same specimen, whereas the results using different specimens, regardless of material, showed greater scatter. The repeatable buckling loads obtainable with mylar specimens was considered of paramount importance for the principal objective of determining whether the critical collapse pressure is sensitive to rate of application of that pressure.

A. Test Program

The actual test program can be detailed as follows:

1) With a dead-weight, high-inertia axial load, the critical values of external pressure that caused collapse were compared for the two cases of slow and fast rates of loading.

2) The above tests were repeated with a low-inertia, pressure-actuated axial loading to determine if the inertia of the axial load was significant.

3) Tests were also conducted with oscillating pressures. Structural resonances were noted as were combinations of frequency and peak pressures inducing collapse of the shell.

These objectives were supplemented, once it was decided to use the electrostatic-loading techniques, by the demonstration and evaluation of this new method of dynamically loading structural models.

B. Test Results

The shell studied experimentally in this program was a mylar shell with a length of 8 inches, a radius of 4 inches and a thickness of 0.005 inch. The axial loads applied before superimposing the radial pressure were between 20 and 30 pounds and the imperfections were such that collapse due to pure end load would occur at values only slightly higher than these loads rather than at the classical value of 70 pounds.

The experimental results showed no significant difference in the critical buckling pressures when the rate of application of the overpressure was changed from one that was too slow to a rate that was adequate to excite a large dynamic overshoot of the ring-mode response. This result was also true when the axial load was changed from a dead weight having high inertia to the low-inertia end cap.

Although the above experimental results do not substantiate the hypothesis that the dynamic buckling pressure can be smaller than the static value, neither do they conflict with the theoretical results described in Section III. For a smaller collapse pressure under dynamic excitation, the theoretical results are interpreted as requiring that the structure have a "tuned" mode with a dynamic buckling pressure that is smaller than the static buckling pressure for the mode in which the shell buckles

statically. The specimen tested experimentally did not satisfy this requirement. Consequently, the experimentally determined absence of a dynamic effect is consistent with, although it does not constitute verification of, the theory.

Before proceeding to discuss the details of the experimental program, it is noted that the electrostatically-applied oscillating pressure permitted the detection of pure structural resonances in a vacuum environment. Acoustic excitation, on the other hand, produces standing-wave resonances of the cavity which are difficult to distinguish from the true structural modes. These oscillatory pressure tests have thus demonstrated another capability of the electrostatic drive system, but the method is not considered fully developed in its potential for various time and spatial distributions of loading.

C. Development of Experimental Techniques

Experimental support during this program required development of a pressurization system that would provide a very high rate of loading. As noted in the opening discussion of the experimental program, it was decided to apply the pressure electrostatically. The required techniques include the application of electrodes to the surfaces being loaded, the arrangement of driving plates, the elimination of air loading that might impede the structural responses, and the provision of d-c and a-c power to control the electrostatic loading of the structure.

The first electrostatic drive system designed was a three-plate, so-called "push-pull" arrangement, as shown in Figure 9. This system was assembled before its supposed advantages were found lacking on completion of the analysis briefly outlined in the Appendix. Inability to observe the specimen was a price considered warranted only if an electrostatic pressure nearly constant with displacement could be produced over a large portion of the annular gap between the fixed outer electrodes. Since the system did not appear to be acting as a "push-pull" system at all, an electrode was attached to a balance and arranged to be driven by either the single-ended or the "push-pull" method. The single-ended system performed as expected; but the three-plate system failed to provide a nearly constant force over any portion of gap between the outer electrodes.

The above mentioned analysis then showed this indeed to be the case. Since neither method could provide the desired constant force, the simpler single-ended system shown in Figure 10 was chosen for further development and for use in the experiments. In Figure 11, the final specimen assembly is shown with dead-weight axial load, adjustable stops for controlling the head travel during collapse, and a lifting mechanism for raising the specimen head when operating inside a vacuum system.

The electrostatic loading rate is controlled by the time constant of the specimen capacitor in series with a resistor inserted in the line through which the capacitor is charged when it is switched across a d-c power supply. The specimen capacitor in parallel with stray capacitance was low enough to allow the series resistance to damp out all oscillation due to line inductance while still keeping an adequately short time constant. On closure of the charging switch, the specimen voltage, V, rises exponentially to 63 percent of the terminal voltage in the time-constant period; since the generated force is proportional V^2, the loading force reaches 40 percent of its terminal value in this time. In the specimen assembly, the combined capacitance being charged was 0.00046 μf. The series charging resistor for rapid loading was 0.1 megohm to give a time constant of 46 microseconds for the fast rate of loading. Changing the resistor to 21 megohm gives a 9700 microsecond rise time and this was used for the slow loading rate. After development of a non-arcing charging switch, it was possible to confirm this charging time by measuring the charging current as shown in Figure 12. The circuit used in applying the pressure is given in Figure 14.

Although the rate of application of the elctrostatic forces can be quite fast, the effective structural loading follows this rate only if the air surrounding the specimen is sufficiently rarefied to prevent buildup of an opposing pressure due to the effective mass of the surrounding air. A moderate vacuum of the order of 10^{-3} mm of mercury absolute pressure is adequate to prevent excess back pressure; diffusion pump techniques producing absolute pressures of about 10^{-5} mm of mercury were necessary, however, to prevent electrical breakdown in the pressure of the outgasing of the mylar specimen and the other materials used in the test apparatus. The electrical breakdown difficulties were solved with

the aid of a materials and spacing model that was tested in the vacuum chamber before the final apparatus shown in Figures 9 and 11 was constructed.

The specimens were prepared as butt-welded mylar cylinders with a vacuum deposited aluminum coating on the inside of the cylinder. The ends were embedded in rings with a low temperature bonding alloy. The lower end ring was fastened to a very heavy plate serving as the vacuum chamber table and the upper ring had supplementary ring weights fastened on during the tests with deadweight, high inertia axial loading. Axial loading was also applied to the top ring with a thin pressure chamber as shown in Figure 13. A calibration of specimen condition was obtained by slowly loading the top cap with lead shot until collapse occurred. At lower axial loads, calibrations were also obtained by slowly applying a differential air pressure.

The oscillating pressure was applied to the shell structure by means of the circuit shown in Figure 15. To avoid frequency doubling and extreme distortion, the a-c drive was superimposed on a d-c bias to apply one polarity of varying magnitude. Since the force varies as the square of the voltage, the resulting oscillating force has sharper peaks than the sinusoidal voltage change and is characterized by a sinusoidal oscillation with 50 percent second harmonic distortion.

With a controlled driving voltage, the electrostatic loading system is extremely versatile for use in performing investigations of the dynamic behavior of structures. By varying the electrode spacing and area, this system offers the potential for controlling the spatial distribution of forces applied to structural surfaces. The forces are limited, however, and attempts to improve this situation lead to problems with charges held on multilayered dielectrics. Since the electrostatic loading system will operate in a vacuum, it can provide structural loading in the absence of any heavy fluid in contact with the structure. This feature, in combination with the capability of applying a load in a few microseconds, warrants the consideration of electrostatic loading for investigations of the dynamic response of structures.

D. Test Procedure and Results

The test specimens were 8 inch diameter by 8 inch long cylindrical shells made of 0.005 inch thick mylar loaded axially and then subjected to an axisymmetric radial overpressure. The radial pressure was developed by the electrostatic attraction force between the two plates of a capacitor when it is charged by connecting it to a source of high voltage. One plate of the capacitor was an aluminum film that was vacuum deposited on the inside of the mylar specimen; the other plate was an inner aluminum cylinder concentrically spaced a short distance from the specimen plate and insulated from it. The loading rate for the pressure was changed from very high to very low values and back by changing a resistor which controlled the time required for the specimen capacitor to be charged up to the potential of the high voltage supply.

A typical test sequence for a given loading rate consisted of 1) raising the supply voltage to some desired load test value while the specimen is held at zero potential with a shorting circuit (position 1 of S_1 in Figure 14), 2) switching the specimen capacitor across this preset source of potential (position 2) so that it is charged through the rate controlling resistor (for 46 or 9,700 microsecond time constant) and held at the voltage controlled radial pressure for three seconds, and 3) switching back to position 1 to release the pressure while the supply voltage is being raised to a higher value for the next shot. The sequence was repeated at 30 second intervals with higher and higher voltage settings until specimen collapse occurred. With no change other than altering the resistor controlling the loading rate, the sequence was then repeated for comparison of the voltages required to cause collapse. The detailed results are briefly given below.

1. Dead-Weight Axial Load with Radial Pressure Steps

Preliminary tests were initially made at atmospheric pressure and later in the vacuum chamber. Under pure axial, the specimen collapsed under loads ranging from 30.50 to 35.07 pounds. At an axial load of 28.48 pounds, the first collapse under electrostatic loading was obtained by slowly raising the d-c voltage across the specimen capacitor to 10 kilovolts. However, a repeated test did not produce a collapse even with the voltage raised to 20 kilovolts. Application of the voltage in steps was then established as the test procedure for the slow, as well as the fast, loading. The first series of tests for which a comparison can be made between slow loadings (9700 microsecond time constant) and a fast loading (46 microsecond time constant) is summarized below.

Series 1	Description	Collapse Pressure, kilovolts	
Test No.		Fast Loading Rate	Slow Loading Rate
1	At atmospheric pressure, with slow loading rates, and with a 28.48 pound axial load, the a-c voltage was applied in steps of 4, 6, 8, 9, 10, etc., kv until collapse occurred at		10
2	With a 28.57 lb axial load, collapse occurred at		12
3	at		12
4	at		11
5	at		13
6	and at		15
7	In the vacuum chamber, with the fast loading rate, repeated Test 1 for collapse at	16	

The collapse in the vacuum chamber terminated in a 1-vertical by 9-circumferential wave pattern that could not be released from contacting the inner electrode with the lifting mechanism. The above comparison made vacuum conditions for both the slow and the fast loadings appear warranted.

Due to specimen deterioration, axial loading now caused collapse at 22.34 and 23.89 pounds, and a new dead-weight load of 22.81 pounds was prepared for the continued tests as follows:

Series 2	Description	Collapse Pressure, kilovolts	
Test No.		Fast Loading Rate	Slow Loading Rate
1	In vacuum and with a 22.81 lb axial load, the d-c voltage was applied in steps of 4, 6, 8, 10, 12, 13, 14, 15, etc. kv until collapse occurred at		14
2	Repeated 1 for collapse at		12
3	and at		13
4	Repeated 1 for collapse at	13	
5	at	12	
6	and at	13	
7	Counterbalanced for overnight rest without axial load. At atmospheric pressure, repeated 1 for collapse at		14
8	at		15
9	and at		15
10	Started vacuum pump and lowered pressure until a vacuum-condition tester* required 30 kv before electrical breakdown. Repeated 1 for collapse at (Specimen stuck to inner electrode and therefore required releasing the vacuum)	10	

*3/8 inch spark gap with 1/32 inch radius tip facing a flat plate.

Series 2		Collapse Pressure, kilovolts	
Test No.		Fast Loading Rate	Slow Loading Rate
11	To the check effects of vacuum pump vibration, atmospheric pressure tests were made with the pump shut down for collapse at		8
12	at		8
13	and at		8
14	Repeating above test at atmospheric pressure but with pump running against a stopped line, collapse occurred at		8
15	at		8
16	and at		8

A deterioration of the specimen is noted in the above series of tests but the first six shots show no significant difference between fast and slow loading rates.

Since buckling appeared stabilized at the lower voltage, fast and slow loadings were run in the vacuum chamber as follows:

Series 3	Description	Collapse Pressure, kilovolts	
Test No.		Fast Loading Rate	Slow Loading Rate
1	Repeated test as in Series 2 No. 1 for collapse at		8
2	and at		8
3	Repeated 1 for a collapse at	8	
4	at	6	
5	at	6	
6	at	8	

Series 3 Test No.	Description	Collapse Pressure, kilovolts	
		Fast Loading Rate	Slow Loading Rate
7	On another pumping cycle necessitated by specimen clinging to inner electrode, repeated 1 for collapse at	8	
8	Repeated 7 for collapse at	8	
9	and at	10	
10	On the final vacuum cycle before the failure of this first specimen the 22.81 pound axial load was retained and the d-c voltage was applied in steps of 2, 4, 6, 8, 9, etc., kv, until collapse occurred at		8
11	at		9
12	at		9
13	at	9	
14	at	9	
15	at	9	
16	at	9	
17	at		9
18	at		9
19	at	9	
20	at	9	
21	and at	9	
22	Continuing as at 10 above but with closer steps of 8 and 8.5 kv, collapse occurred at	8.5	
23	at	8.5	
24	at	8.5	
25	at		8.5
26	at		8.5
27	and at		8.5

This series of tests again shows no variation in results during repetitive tests with no change other than that of altering the charging resistor for either the fast or slow pressure-loading rate. For this specimen and loading condition, it is concluded that there is no decrease in the critical collapse pressure under a loading rate high enough to excite the axisymmetric ring mode.

2. Axial Force on Low-Inertia End Cap with Radial Pressure Steps

The equipment was altered by changing the dead-weight, high-inertia axial load to a low-inertia end ring in which the axial force is developed with a large-diameter, thin pressure chamber. The specimen collapsed with a pure axial load due to a 3-pound end mass and air pressure equivalent to 17.1 inch of Convoil-20 (specific gravity 0.865) applied to the pressure chamber. The axial-loading air pressure was reduced to 16.2 inches during the following series of tests.

Series 5	Description	Collapse Voltage, kilovolts	
Test No.		Fast Loading Rate	Slow Loading Rate
1	During the first vacuum cycle and with the axial load indicated above, the d-c voltage was applied in steps of 4, 5, 6, etc., kv, until collapse occurred at		8
2	and at	8	
3	Repeated 1 (2nd vacuum cycle) for a collapse at	7	
4	at		9
5	at	9	
6	at		9
7	at	9	
8	and at		9

Series 5		Collapse Voltage, kilovolts	
Test No.		Fast Loading Rate	Slow Loading Rate
9	Repeated 1 (3rd vacuum cycle) for a collapse at		8
10	at	8	
11	at		8
12	at	8	
13	at		10
14	at	10	
15	at		10
16	and at	10	
17	Repeated 1 (4th vacuum cycle) for a collapse at	8	
18	at		11
19	at	10	
20	and at The aluminum coating began to peel off the mylar specimen near the end of this cycle.		11

For the low-inertia axial loading condition, no significant difference in the critical collapse pressure is found due to a high pressurizing rate.

3. Dead-Weight Axial Load with Oscillatory Pressure

An oscillating radial pressure was obtained by applying a d-c voltage with superimposed a-c having an amplitude that was equal to or less than the d-c value. This pulsating potential of one polarity, produced a pulsating inward radial force on the thin mylar shell. It was varied in frequency and amplitude to find various combinations causing collapse of the structure. The results were not sufficiently consistent during eight

vacuum cycles to establish a detailed description of the behavior but it is significant that collapse was obtained at peak potentials both below and above the current d-c step voltages causing collapse. This is consistent with results obtained in Reference[1].

By direct transmission through the walls of the vacuum chamber, resonant frequencies of the driven cylindrical specimen were detected. The low pressure of about 10^{-5} mm of mercury allowed this detection of structural resonances without the influence of cavity resonances of a gas-filled chamber. With a 27.19 pound dead-weight axial load (about 95 percent of the maximum allowable) on the 8-inch diameter by 8-inch long cylinder made of 0.005 inch mylar, resonances were detected at 73, 83 (strong), 94, 105, 120, 162 (strong), 183, 210, 246, 317, 472, 800, 890, 1190, 1270, 1500, 1860, 2130, 2330, 2550, 2670, 3030, 3180 (strong), 3330, 3500, 3640, 4030, 4320, 4600, 4830, 5000, and 5580 cps.

V. CLOSING COMMENTS

It is to be noted that all objectives of the study have been achieved. The existence of "dynamic buckling" has been explored both by a theoretical analysis and a laboratory test program. Solution of the usual nonlinear shallow shell equations has lead to the conclusion that in a set of somewhat restricted circumstances, it may be possible to buckle an axially-loaded cylindrical shell at a pressure smaller than the static buckling value if the pressure has a sufficiently fast rate of loading.

Experiments have failed to detect such a difference in buckling pressures, but these tests could only be conducted on cylinders that theory predicted would not show the desired effect. Since it was necessary to pursue both the theoretical and experimental programs simultaneously, this state of affairs was not realized until the closing stages of the entire program; well after commitments had to be made on the experimental program.

The concept of electrostatically loading a structural model for experimental dynamic response studies has been proven feasible and is certainly worthy of further study. As with any new technique, however, there are limitations and unexpected difficulties. There is a maximum voltage at which one can operate and this, of course, places limits on the pressures that can be generated and consequently on shell configurations that can be tested. Because of these limitations, it was not possible to test the thicker shells that theory indicates should show a dynamic effect. Even though the test results that were obtained were consistent with theory, the theory still lacks positive confirmation.

Additional avenues for theoretical studies can also be suggested. Evensen in[24] mentions that in his work with rings there is a strong tendency for the nonlinear vibration of one "breathing" mode to couple with another when the amplitude is larger than a critical value. Perhaps a three-mode study (ring mode plus two breathing modes) may prove interesting. Damping is a quantity that is present in all structures but its effect was not included in this study because of the viscoelastic nature of the damping in mylar cylinders. However, an appraisal of its effects would be of some interest. Most likely, the effect of damping would

reduce the dynamic effect by increasing the dynamic buckling pressures in a fashion analogous to the damping (iso-μ) effect on the Mathieu stability diagrams. A third possible modification would be the inclusion of the variation in electrostatic force with displacement.

ACKNOWLEDGEMENTS

The authors happily express their indebtedness to NASA for supporting this work, to Dr. M. V. Barton, Director of the Engineering Mechanics Laboratory, Professor Y. C. Fung and Professor E. E. Sechler for their encouragement, suggestions and assistance throughout the program; and to Mr. D. A. Evensen for his assistance in checking the derivation of the differential equations and for his many timely and valuable comments. The help of Mr. R. N. Schreiner with the numerical computations and of Dr. W. G. Gottenberg with the experimental apparatus is also acknowledged.

APPENDIX

ANALYSIS OF ELECTROSTATIC DRIVE SYSTEMS FOR DYNAMICALLY LOADING STRUCTURAL SURFACES

When the two-plate, single-ended and the three-plate, so-called "push-pull" electrostatic drive systems are given the same plate spacing and allowed the same maximum potential difference that might cause electrical breakdown, analysis of these systems as parallel-plate capacitors indicates that they produce the same value of a step-function in force and that neither system produces a force that is at any point insensitive to a change in the spacing. This analysis has shown that the "push-pull" system does not produce a nearly constant electrostatic pressure over a relatively large portion of the total annular gap between the fixed electrodes as first predicted. This prediction was based on the literature dealing with electrostatic loudspeakers and on the implications of the term "push-pull." The force on a small isolated test charge is, in fact, constant throughout a uniform electrostatic field. But when the charge isolated on the central plate of the three-plate electrostatic loading system is of sufficient magnitude to produce the required step-function loading when the outer plates are connected to an allowable potential difference, the determination of the variation in force with displacement of the specimen plate must take into account the capacitance variation on each side of the plate and the effect of the induced charges. This results in a linear force variation of considerable magnitude during the excursion of the center plate.

The above results are derived from the basic equation for the electrostatic force on the surface of a conductor. On such a surface carrying a charge σ per unit area, there is an outward force per unit area[31, 32]

$$f = \frac{\delta \sigma^2}{2\epsilon} \tag{A1}$$

where ϵ is the absolute permittivity of the medium outside the conductor and δ determines whether the system of units[33] used is rationalized such that the π terms are contained in the equations for problems dealing with circulary symmetry rather than with rectangular configurations. The

direction of the force is always outwards; there is consequently never a push against the surface of a conductor. This equation suggests that the term "push-pull" is somewhat inappropriate when applied to any system designed to apply a step-function or steady single-direction force to a structure by electrostatic means.

In Equation (A1), the absolute permittivity ϵ is given by

$$\epsilon = \epsilon_o \epsilon_r \tag{A2}$$

where ϵ_o is the absolute permittivity of free space, i.e., in a vacuum, and ϵ_r is the relative permittivity or dielectric constant of the medium adjacent to the conductor. These dimensionally homogeneous equations are applicable for any consistent system of units. In air at one atmosphere, $\epsilon_r = 1.0006$; and for the unrationalized electrostatic C.G.S. system of units (e.s.u.), $\delta = 4\pi$, $\epsilon_o = 1$, σ is in e.s.u. of charge per cm^2, and the force per unit area is in dynes per cm^2.

In considering the means of obtaining the charge density σ, we make use of the definition of the capacitance between two conductors

$$C \equiv Q/V \tag{A3}$$

where V is the potential difference between the two conductors and Q is the charge carried by either conductor, i.e., + Q on one conductor and -Q on the other.[34] For the parallel-plate capacitor of uniform separation, the charge Q is evenly distributed over the area A, the surface density of charge on either conductor is then

$$\sigma = Q/A \tag{A4}$$

and the capacitance is[35]

$$C = \epsilon A/\delta t \tag{A5}$$

where t is the separation distance between the closely spaced portion of the conductors. From the above relations, we then obtain the attraction force per unit area between the plates of a uniformly spaced parallel-plate capacitor as

$$f = \frac{\epsilon V^2}{2\delta t^2} \qquad \text{(A6)}$$

In using these additional dimensionally homogeneous equations with the consistent electrostatic C.G.S. system of units (e.s.u.), Q is in e.s.u. of charge (1 e.s.u. charge unit = 3×10^{-9} Coulombs), V is in e.s.u. of potential difference = 300 volts), A is in cm^2, t is in cm, C is in e.s.u. of capacitance (1 e.s.u. of capacitance = 9×10^{-11} Farads), and again the force per unit area is in dynes per cm^2 (1 dyne per cm^2 = 1.45×10^{-5} psi).

We can convert the basic force equation to one using a particular choice of practical units and obtain the attraction force between the plates of a uniformly spaced parallel-plate capacitor as

$$P = 0.994 \times 10^{-12} \frac{E^2}{d^2} \qquad \text{(A6a)}$$

where P is in psi, E is the potential difference between the plates in volts, and d is the plate separation in inches. This equation is not dimensionally homogeneous and is valid only for the stated units.

In the application of Equations (A1) through (A6) to electrostatic loading systems, it is constantly recognized that the conductor plates have two sides and that the outward surface forces on both sides must be determined to evaluate the net electrostatic loading on the structure. With the specimen forming or supporting the center plate conductor of a three-plate electrostatic drive system, the capacitance and forces on both sides are significant in magnitude and the structural loadings is the difference between the forces on the two surfaces of the conductor. With the speciment as one conductor of a two-plate system, the capacitance between the plates will likely predominate to such an extent that the capacitance to earth and the outward force on the exterior face of the conductor is negligible. Also, as in the design shown in Figure 10, it may be possible to make this exterior force zero by keeping the specimen plate at ground potential.

SYMBOLS

A_0, A_1, A_2	Constants, see Equation (5)
$B_1, B_{\pm 1}, B_3$	Constants, see Equation (5)
C_1, C_2	Constants, see Equation (5)
$c = \frac{1}{R}\sqrt{E/\rho}$	Circular frequency of ring mode
$D = Eh^3/12(1-\nu^2)$	Shell flexural rigidity
E	Young's modulus
F	Stress function
f	Electrostatic force
$G_1, \cdots, G_7$	Constants, see Equation (12)
h	Wall thickness
$K_1, \cdots, K_7$	Constants, see Equation (12)
$k = h^2/12R^2$	Nondimensional thickness parameter
L	Length of shell
$\ell = L/R$	Nondimensional shell length
m	Number of axial half-waves in breathing mode
$N_1, N_{\pm 1}, N_3$	Constants, see Equation (5)
N_y, N_x	Shell membrane stress resultants, Equation (6)
n	Number of circumferential waves in breathing mode
P	Axial load
p	Lateral pressure
p_{cr}	Critical pressure, pressure at which buckling occurs
$p(\tau)$	Pressure-time (nondimensionalized) history
R	Radius of shell
T	Kinetric energy, Equation (9)

SYMBOLS (Continued)

t	Time
U	Strain Energy, Equation (11)
u_1	Initial asymmetric component of radial deformation (nondimensionalized to thickness)
u, v, w	Shell displacement coordinates
w_I	Initial state of deformation
x, y	Shell coordinates
W_A	Work done by axial force, Equation (14)
W_p	Work done by lateral pressure, Equation (13)
V	Voltage
$a_1, \cdots, a_5$ $\beta_1, \cdots, \beta_6$ $\gamma_1, \cdots, \gamma_7$	Constants, see Equation (16)
δ	Constant, see Equation (26)
ϵ	Absolute permittivity
η	Constant, see Equation (25)
ν	Poisson's ration, taken as $\nu = 0.3$
ρ	Mass density of shell material
σ	Charge density
σ_{x_o}	Initial axial stress
$\tau = ct$	Nondimensionalized time
τ_1	Rise time for ramp-step pressure
τ_2	Duration of impulsive pressure
Ω_0	Frequency parameter for ring mode, Equation (16)
Ω_1	Frequency parameter for breathing mode, Equation (16)

REFERENCES

1. Engineering Mechanics Laboratory, "Final Report on Buckling of Shells Under Dynamic Loads," STL Report 8622-0001-RU-000, EM 11-22, 26 October 1961, (condensed version to appear in AIAA Journal).

2. A.S. Vol'mir and V.E. Mineev, "An Experimental Investigation of the Buckling of a Shell Under Dynamic Load," Soviet Physics-Doklady, Vol. 125, No. 5, (1959), p. 1002.

3. A.S. Vol'mir, "On the Stability of Dynamically Loaded Cylindrical Shells," Soviet Physics-Doklady, Vol. 123, No. 5 (1958), pp. 806-808.

4. V.L. Agamirov and A.S. Vol'mir, "Behavior of Cylindrical Shells Under Dynamic Loading by Hydrostatic Pressure or by Axial Compression," ARS Journal Supplement (January 1961), p. 98 (Translated from Bull. Acad. Sci. USSR, Div. Tech. Sci, Mechanics and Machine Construction, No. 3, 1959, pp. 78-83).

5. A.N. Markov, "Dynamic Stability of Anisotropic Cylindrical Shells," Prinkl. Mat. Mekh., 13 (1949), pp. 145-150.

6. O.D. Oniashvili, "Certain Dynamic Problems of the Theory of Shells," Translation by M.D. Friedman, Inc., West Newton, Mass., from Press of the Academy of Sciences of the USSR, Moscow, 1957.

7. M.A. Lavret'ev and A. Yu. Ishlinskii, "Dynamic Forms of Loss of Stability on an Elastic System," Doklady Akad. Nauk SSSR, Vol. 64, No. 6 (1949); pp. 779-782. (Translated by R.M. Cooper in STL-TR-61-5110-41).

8. Yu, I. Kadashevich and A.K. Pertsev, "On the Loss of Stability of a Cylindrical Shell Under Dynamic Loading," Izv. AN. Otd. Tech. Nauk, Mekh. 1 Mash., No. 3(1960), pp. 30-33. (Translated by K.N. Trirogoff, and R.M. Cooper, Aerospace Corp.).

9. V.V. Bolotin, "Certain Nonlinear Problems of Dynamic Stability of Plates," Izv. Akad. Nauk SSSR, No. 10 (1954).

10. V.V. Bolotin, "Behavior of Thin Elastic Shells in Response to Impulsive Loading," Stroit, Mekhi. Konstructsii, No. 2 (1959), pp. 9-16.

11. E.A. Beilin and G. Yu Dzhanelidze, "Survey of Work on the Dynamic Stability of Elastic Systems," Prikl. Mat. Mekh., Vol. 16 (1952), pp. 635-648 (Translated by K.N. Trirogoff and R.M. Cooper, Aerospace Corp., TDR-930(2119)TN-2, 15 November 1961).

12. V.V. Bolotin, "The Dynamic Stability of Elastic Systems," (Gostekhizdat, Moscow, 1956) Translation by V.I. Weingarten, K.N. Trirogoff, K.D. Gallegas, Aerospace Corp., Translations, TDR-169(3560-30)TR-2 Vol. I, II, III, IV.

13. V.V. Bolotin, G.A. Boichenko, B.P. Markharov, N.I. Sudakova, Y.Y. Shveiko, "Loss of Stability of Thin Elastic Shells Under the Effect of Impulsive Loads," Stroit. Mekh. i Raschet Sooruzhenii, No. 2, 1959, pp. 9-6, (STL Translation No. 72 by Z. Jakubski, 1963).

14. E.I. Grigoliuk, "Nonlinear Vibrations and Stability of Shallow Beams and Shells," Izv. Akad. Nauk SSSR, Vol. 3, 1955, pp. 33-68 (Translation by Institute of Engineering Research, Univ. of California, Berkeley, Applied Mechanics Series 131, No. 7, January 1960).

15. J.C. Yao, "Stability of a (Infinite) Cylinder Under Dynamic Radial Pressure," ARS Journal, December 1961, pp. 1705-1708.

16. J.C. Yao, "The Dynamics of the Elastic Buckling of Cylindircal Shells," Proc. of 4th U.S. National Congress of Applied Mechanics, Vol. I, 1962, pp. 427-432.

17. A.P. Coppa and W.A. Nash, "Dynamic Buckling of Shell Structures Subject to Longitudinal Impact," Tech. Report ASD-TDR-62-774, December 1962.

18. J.C. Yao, "Dynamic Stability of Cylindrical Shells Under Static and Periodic Axial and Radial Loads," AIAA Journal, Vol. 1, No. 6, June 1963, pp. 1391-1396.

19. E.A. Fitzgerald, "The Stability of A Short Cylinder Under Dynamic Radial Pressure," Douglas Missile and Space Systems Report SM-41947, 30 April 1963.

20. J.N. Goodier and I.K. McIvor, "The Elastic Cylindrical Shell Under Nearly Uniform Radial Impulse," ASME Paper No. 63-APMW-6, presented at West Coast Conference of Applied Mech. Division, Monterey, California August 1963.

21. H.E. Lindberg, "Buckling of a Very Thin Cylindrical Shell Due to an Impulsive Pressure," ASME Paper No. 63-APMW-7, presented at West Coast Conference of Applied Mechanics Division, Monterey, California, August 1963.

22. R.S. Roth and J.M. Klosner, "Nonlinear Response of Cylindrical Shells with Initial Imperfections Subjected to Dynamic Axial Loads," RAD-TM-63-43, Avco Corp., 31 July 1963.

23. L.H. Donnell, "A New Theory for the Buckling of Thin Cylinders Under Axial Compression and Bending," Trans. ASME, Vol. 56, November 1934, pp. 795-806.

24. D.A. Evensen, "Some Observations on the Nonlinear Vibrations of Thin Cylindrical Shells," To be published in AIAA Journal.

25. B. Budiansky and R.S. Roth, "Axisymmetric Dynamic Buckling of Clamped Shallow Spherical Shells," Collected Papers on Instability of Shell Structures, NASA TN D-1510, 1962.

26. N.J. Hoff and V.G. Bruce, "Dynamic Analysis of the Buckling of Laterally Loaded Flat Arches," Journal of Mathematics and Physics, Vol. 32, No. 4., January 1954, pp. 276-288.

27. V.I. Weingarten, E.J. Morgan, and P. Seide, "Final Report on Development of Design Criteria for Elastic Stability of Thin Shell Structures," Space Technology Laboratories, Inc., Report No. STL/TR 60-0000-19425, AF 04(647)-619, December 1960.

28. N.W. McLachlan, "Theory and Application of Mathieu Functions," Oxford University Press, London, 1947.

29. R.C. Tennyson, "A Note on the Classical Buckling Load of Circular Cylindrical Shells Under Axial Compression," AIAA Journal, Vol. 1, August 1963, pp. 475-476.

30. D.A. Evensen, "Highspeed Photographic Observations of Buckling of Thin Cylindrical Shells," to be published in Experimental Mechanics.

31. D.H. Trevana, "Static Fields in Electricity and Magnetism," Butterworth and Co., Ltd., London (1961), pp. 102-103.

32. E.S. Shire, "Classical Electricity and Magnetism," Cambridge University Press, Cambridge (1960), pp. 68-71.

33. E.S. Shire, "Classical Electricity and Magnetism," Cambridge University Press, Cambridge (1960), p. 13 and p. 366.

34. D.H. Trevana, "Static Fields in Electricity and Magnetism," Butterworth and Co., Ltd., London (1961), p. 5.

35. D.H. Trevana, "Static Fields in Electricity and Magnetism," Butterworth and Co., Ltd., London (1961), p. 120.

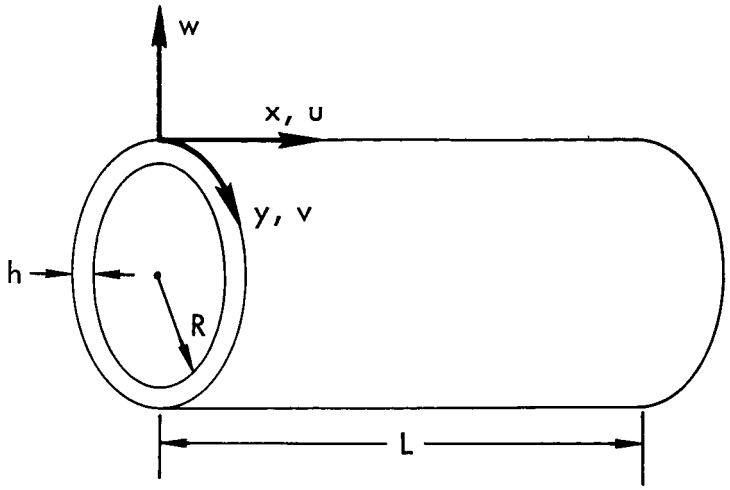

Figure 1a. Coordinate System

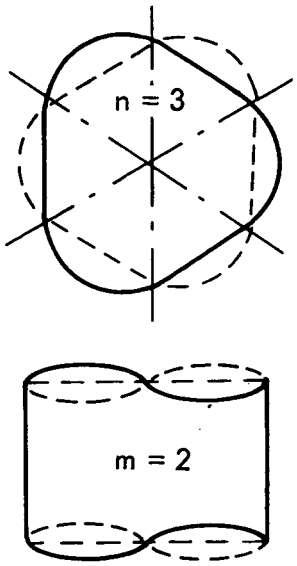

Figure 1b. Typical Breathing Mode m=2, n=3

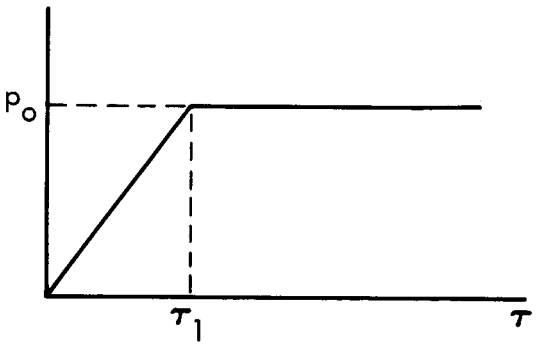

(a) Ramp-Step Pressure

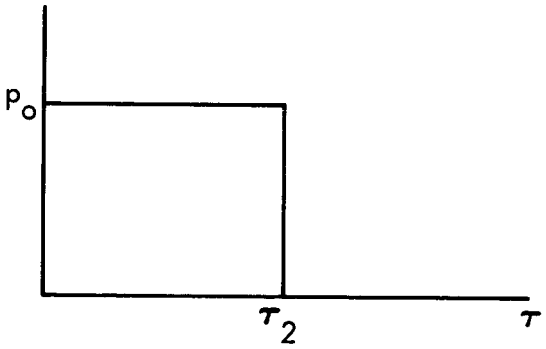

(b) Rectangular Pulse

Figure 2. Pressure-Time Histories

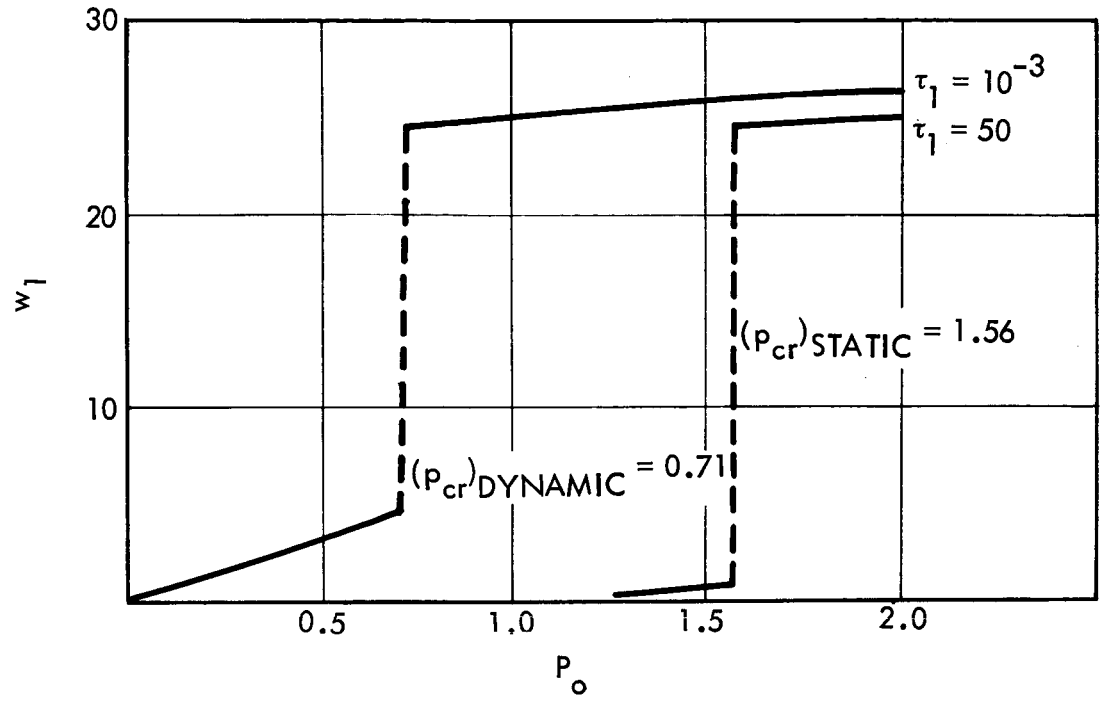

Figure 3. Maximum Deflection For Mode m=7, n=1

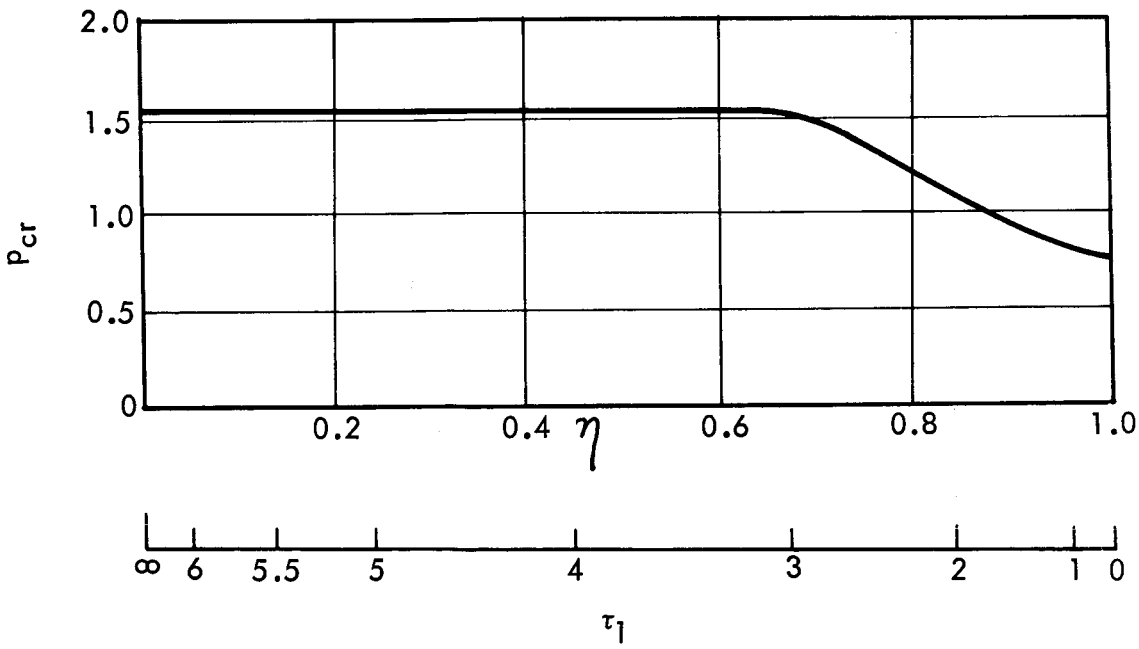

Figure 4. Variation in Critical Pressure With Rise Time for the Mode m=7, n=11

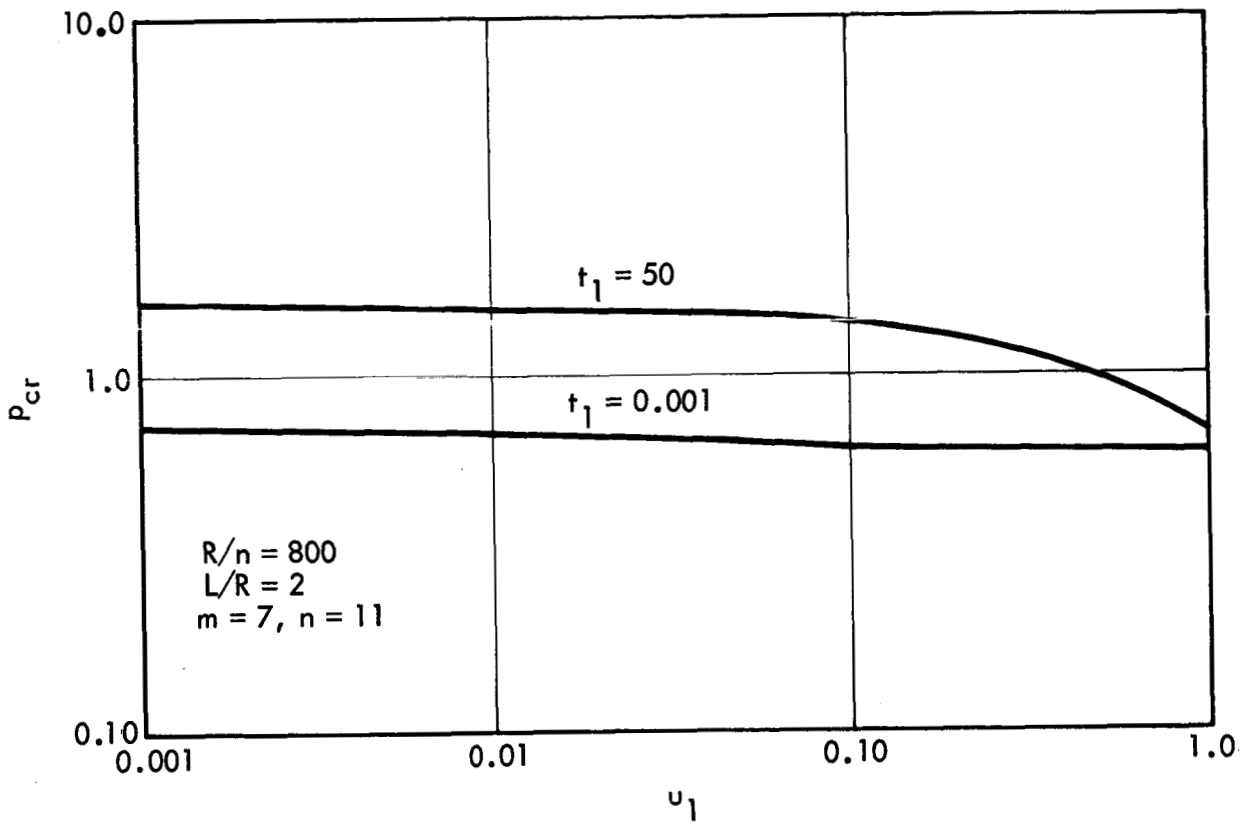

Figure 5. Effect of a Change in Initial Imperfection

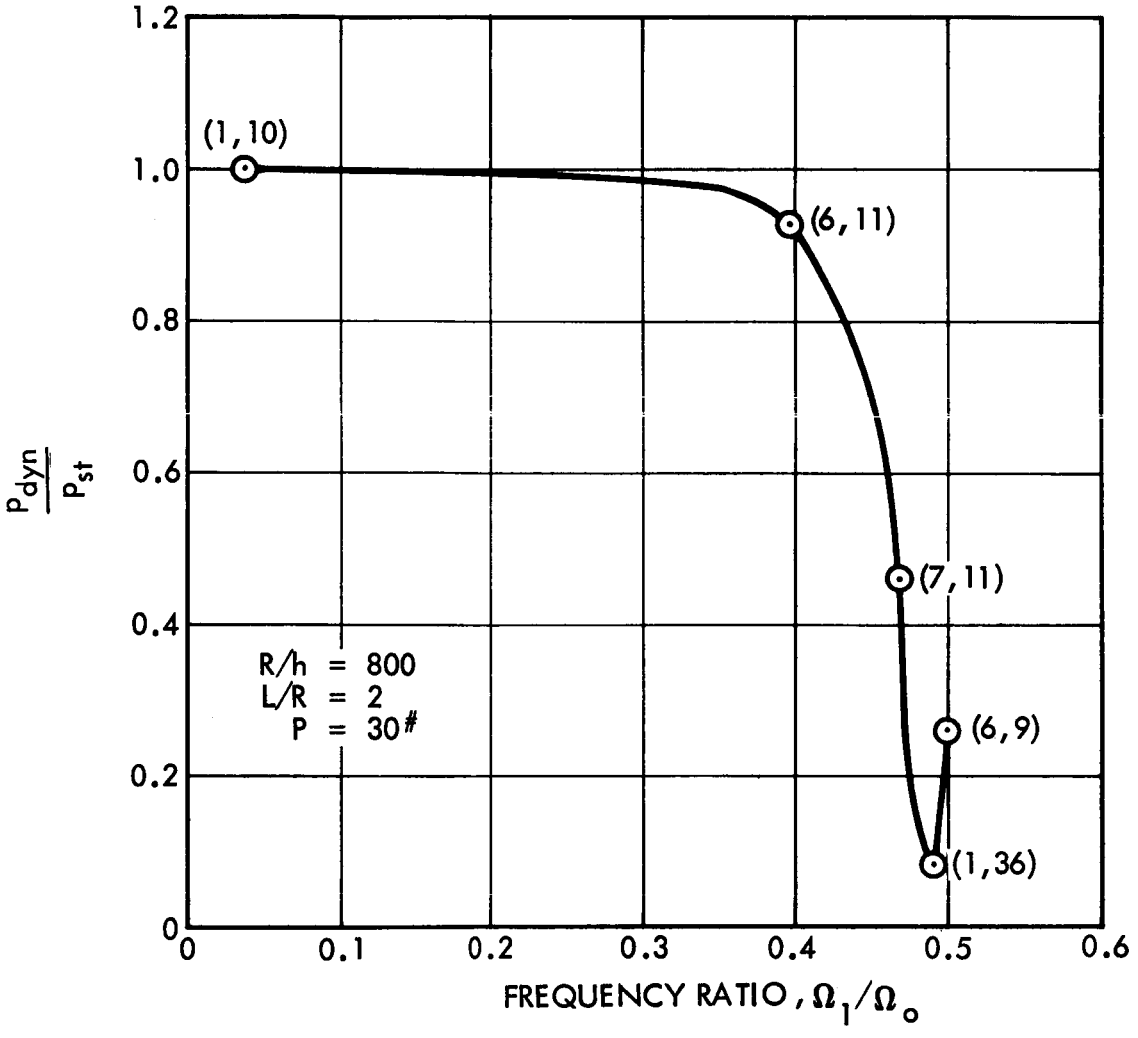

Figure 6. Effect of Tuning Between Breathing Mode and Ring Mode

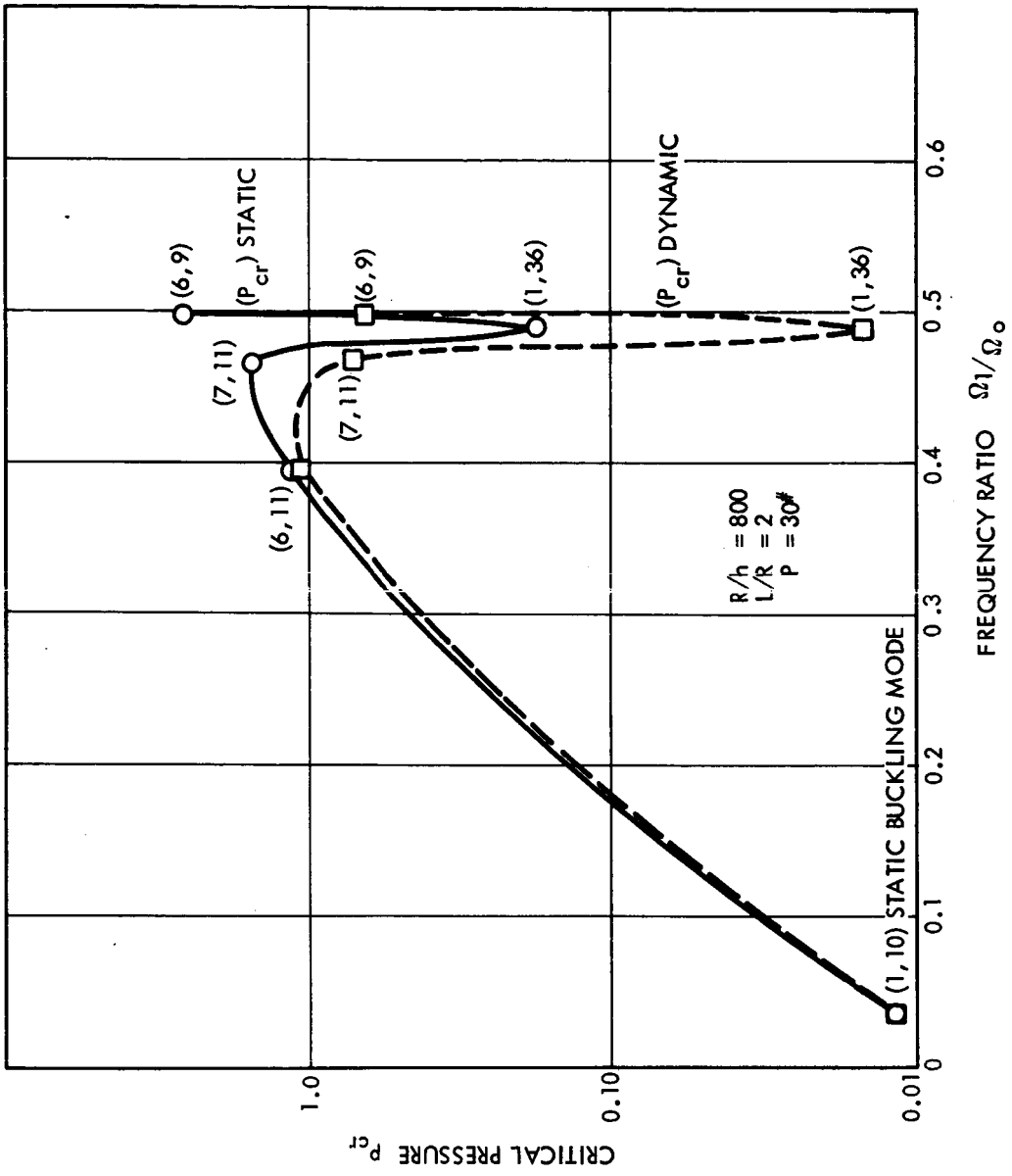

Figure 7. Effect of Tuning on The Dynamic Buckling Pressure

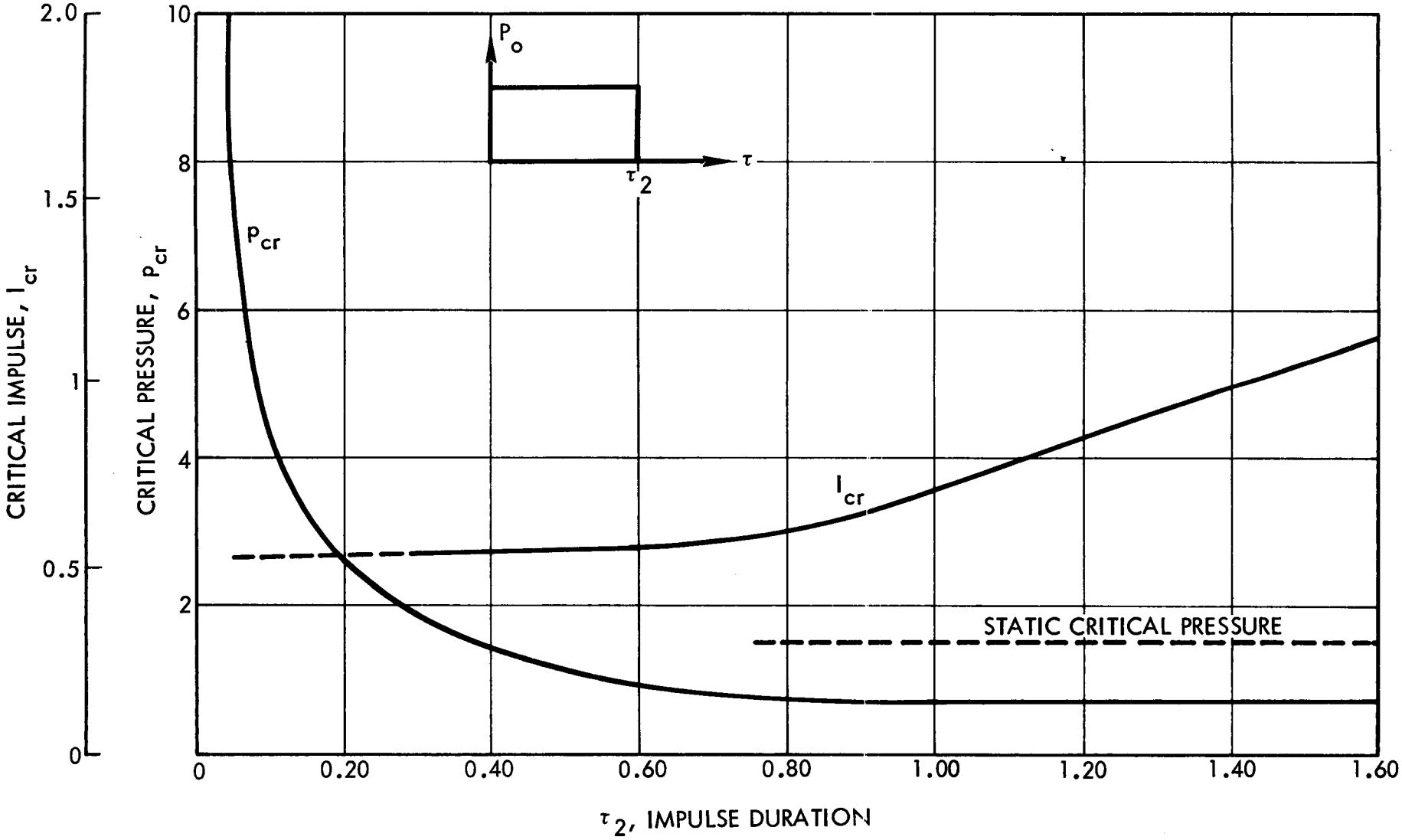

Figure 8. Stability Under Impulsive Pressure R/h = 800, L/R = 2, P = 30 lbs, m = 7, n = 11

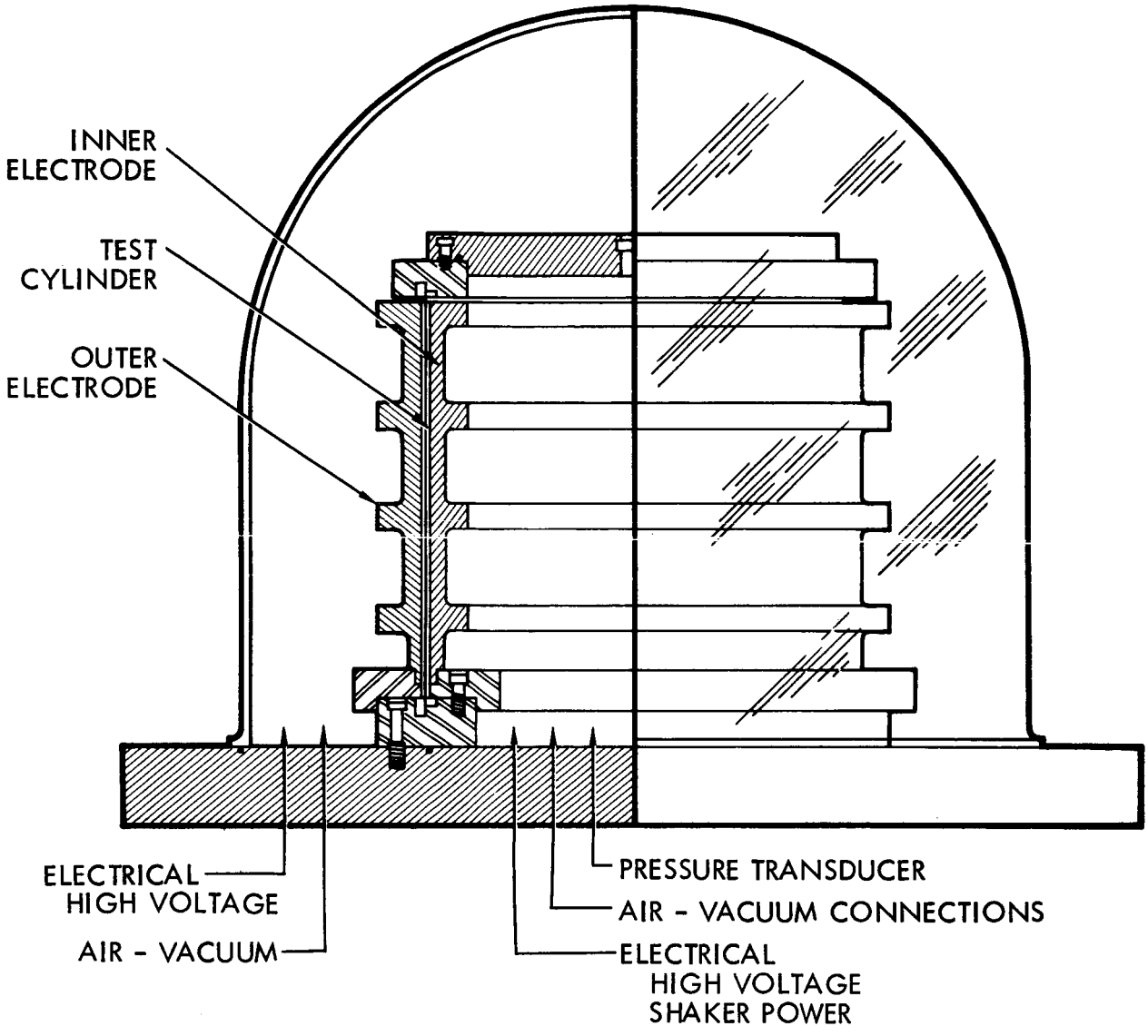

Figure 9. Schematic Cross Section of Developmental Three-Plate "Push-Pull" Electrostatic Loading Apparatus

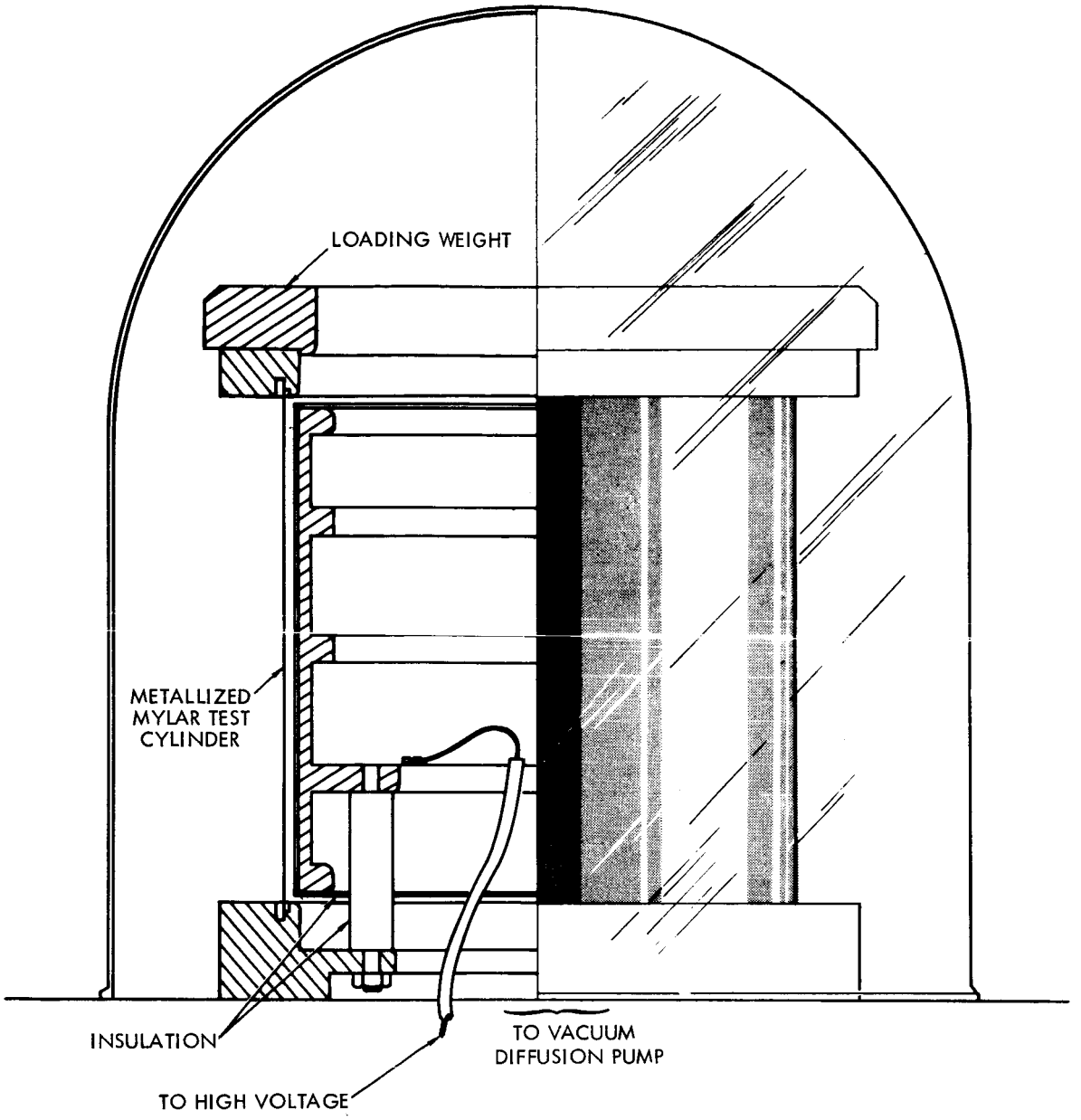

Figure 10. Schematic Cross Section of Two-Plate Electrostatic Loading Apparatus.

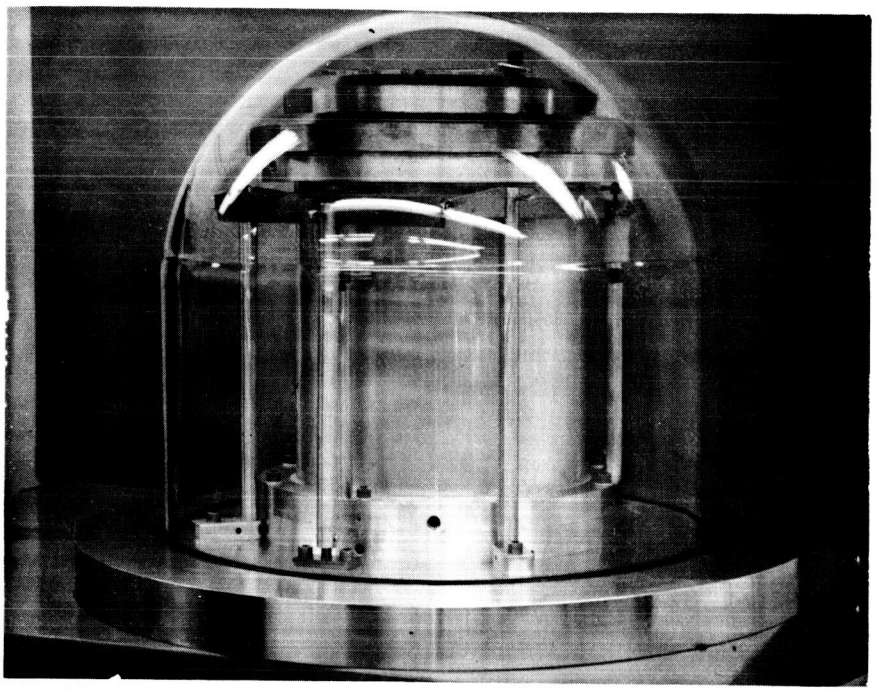

Figure 11. Vacuum System with Two-Plate Electrostatic Loading System

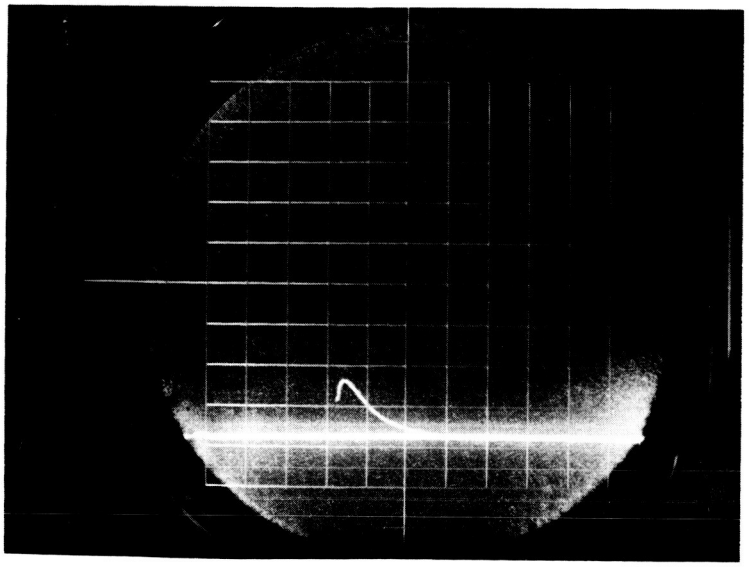

Figure 12. Confirmation of Rapid Loading of Specimen. Charging Current vs Time (50 microseconds per division) shows 45 Microsecond Time Constant

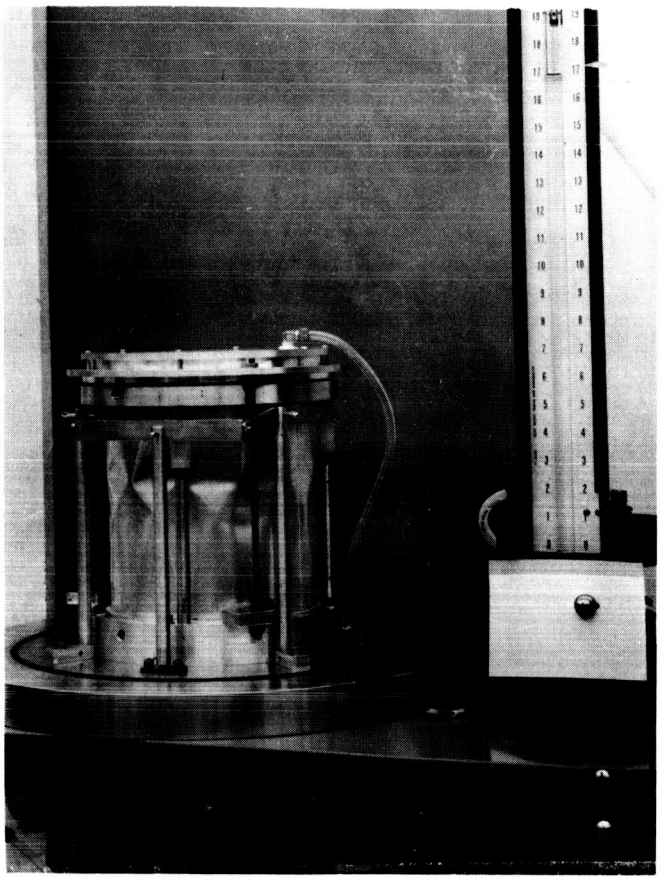

Figure 13. Low-Inertia, Pressure-Actuated Axial Loading System Shown at the Top of a Buckled Cylindrical Shell. Vertical Rods are for Limiting The Extent of Collapse and for Limiting Specimen Cap When Vacuum Belljar is Inplace

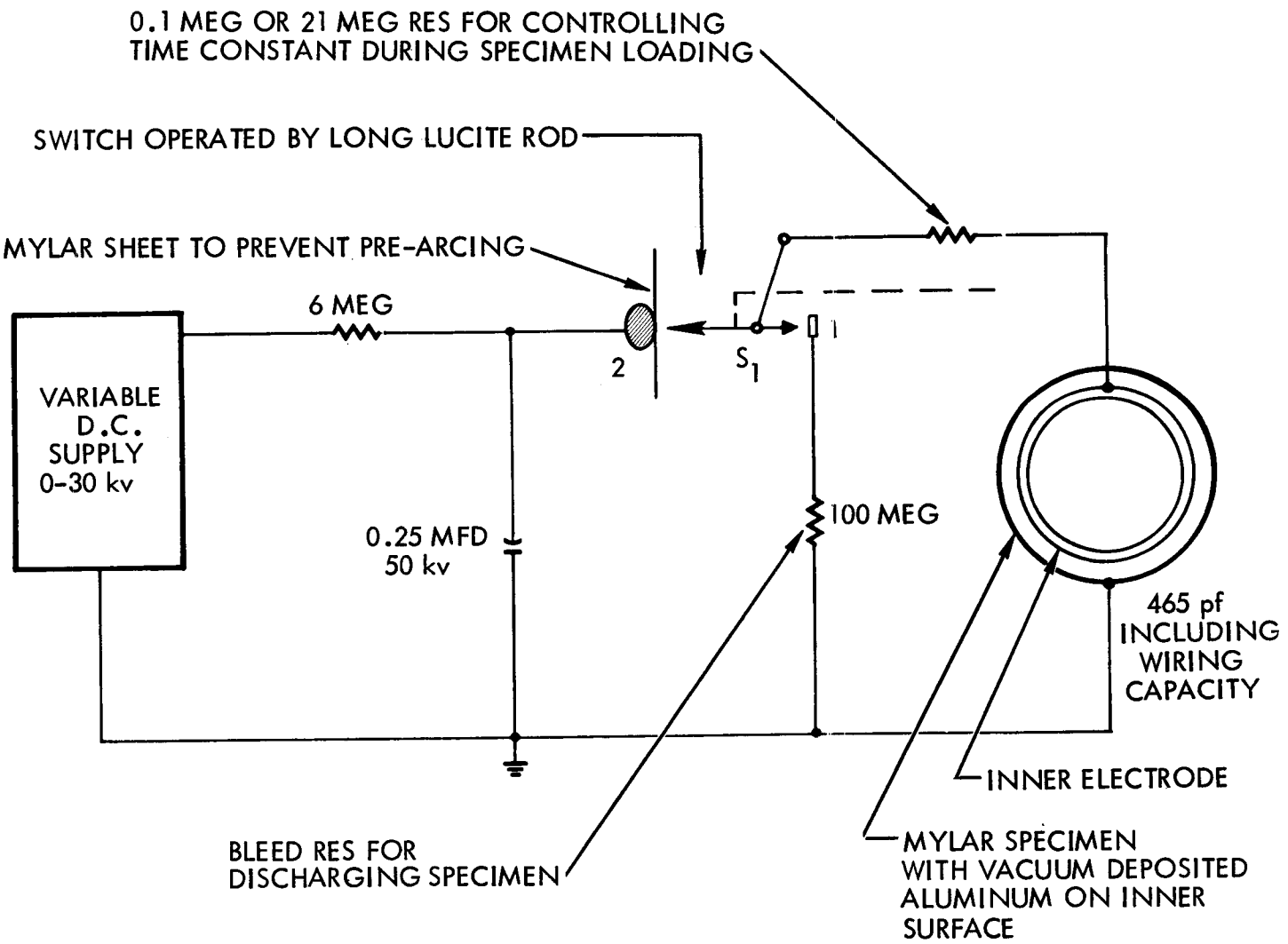

Figure 14. Circuit for Electrostatically Pressure-loading The Specimen at Different Loading Rates

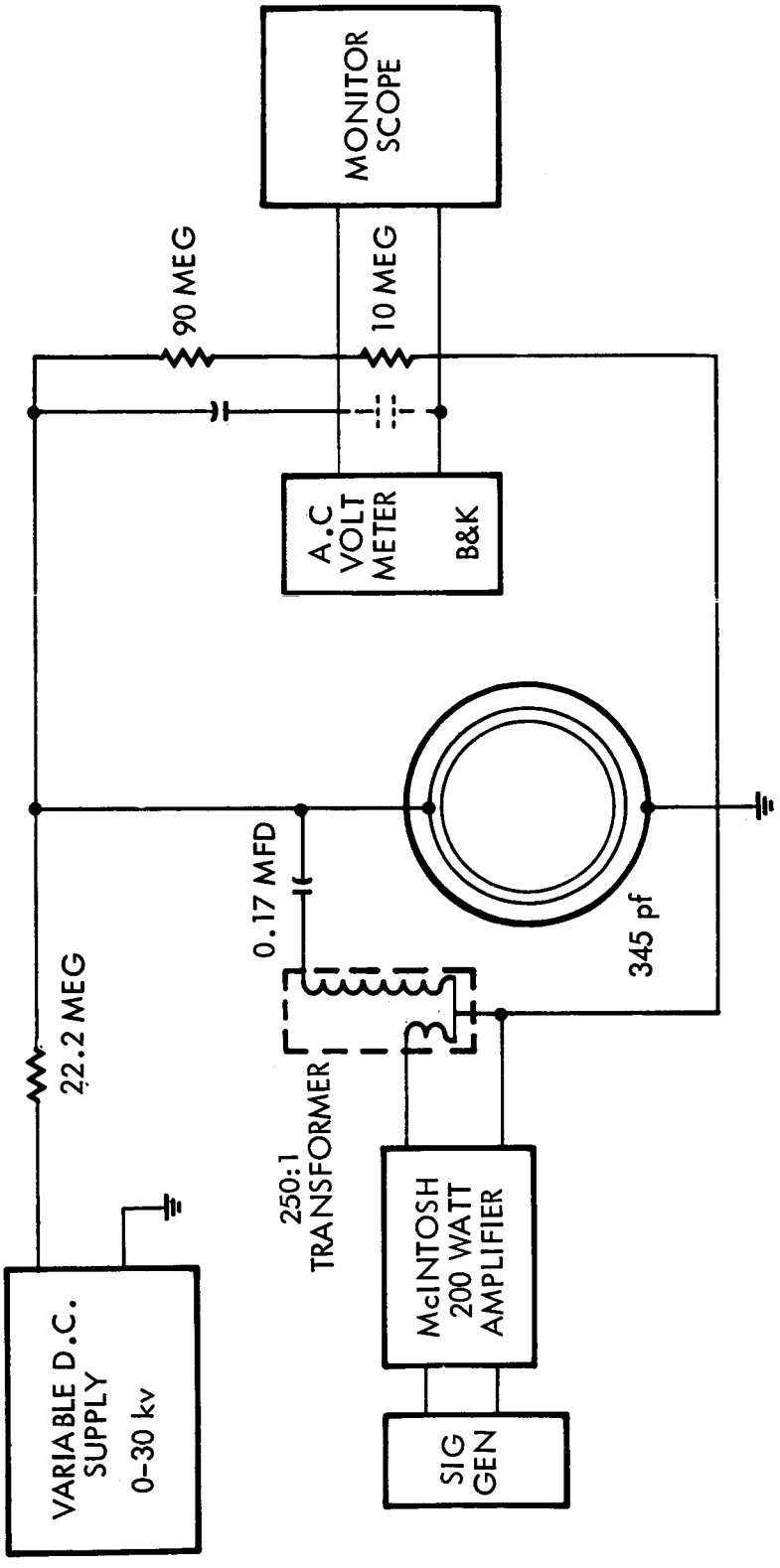

Figure 15. Circuit for Producing an Oscillating Electrostatic Pressure on Specimen